AGU PUBLICATIONS

Paleoceanography and Paleoclimatology

RESEARCH ARTICLE
10.1002/2017PA003228

Key Points:
- The Mediterranean outflow was saltier during the Last Glacial Maximum
- The Mediterranean Sea loses most of its Glacial salt during HS1
- Clumped isotope thermometry can be used to estimate the temperature of Mediterranean Outflow Water

Supporting Information:
- Supporting Information S1
- Data Set S1

Correspondence to:
J. van Dijk,
joep.vandijk@erdw.ethz.ch

Citation:
van Dijk, J., Ziegler, M., de Nooijer, L. J., Reichart, G. J., Xuan, C., Ducassou, E., Bernasconi, S. M., & Lourens, L. J. (2018). A saltier Glacial Mediterranean Outflow. *Paleoceanography and Paleoclimatology*, *33*, 179–197. https://doi.org/10.1002/2017PA003228

Received 3 AUG 2017
Accepted 23 DEC 2017
Accepted article online 25 JAN 2018
Published online 10 FEB 2018

A Saltier Glacial Mediterranean Outflow

J. van Dijk[1], M. Ziegler[2], L. J. de Nooijer[3], G. J. Reichart[2,3], C. Xuan[4], E. Ducassou[5], S. M. Bernasconi[1], and L. J. Lourens[2]

[1]Geological Institute, ETH Zürich, Zürich, Switzerland, [2]Department of Earth Sciences, Utrecht University, Utrecht, Netherlands, [3]NIOZ-Royal Netherlands Institute for Sea Research and Utrecht University, Texel, Netherlands, [4]National Oceanography Centre Southampton, University of Southampton, Southampton, UK, [5]University of Bordeaux, UMR-CNRS 5805 EPOC-OASU, Bordeaux, France

Abstract The state of Atlantic Meridional Overturning Circulation (AMOC) is influenced by both the strength and the location of the Mediterranean Outflow Water (MOW) plume in the Gulf of Cadiz. To evaluate the influence of MOW on AMOC over deglaciations, precise and accurate salinity and temperature reconstructions are needed. For this purpose, we measured Mg/Ca and clumped isotopes of several benthic foraminiferal species at Integrated Ocean Drilling Program Site U1390 in the Gulf of Cadiz. The clumped isotope results of *Cibicidoides pachyderma*, *Uvigerina mediterranea*, and *Pyrgo* spp. are consistent between species and record no significant difference in Last Glacial Maximum to Holocene deep water temperature. Over the deglaciation, the Mg/Ca-based temperatures derived from *U. mediterranea* indicate three periods of MOW absence at Site U1390. Mg/Ca-based temperatures of *Hoeglundina elegans* and *C. pachyderma* are on average 6°C too cold when compared to the present core-top temperature, which we explain by a carbonate ion effect on these epibenthic species related to the high alkalinity of the MOW. Combining deep water temperature estimates with the benthic oxygen isotope data and considering different relationships between seawater oxygen isotopes and salinity, we infer a salinity decrease of MOW by three to eight units over the deglaciation and four units during Sapropel 1, accounting for the global $\delta^{18}O$ depletion due to the decrease in ice volume. Our findings confirm that the Mediterranean Sea accumulates excess salt during a glacial low stand and suggest that this salt surged into the Atlantic over the deglaciation, presumably during Heinrich Stadial 1.

Plain Language Summary The Gulf Stream is slowing down because of the meltdown of the Greenland ice sheet. In the past, such a slowdown often resulted in a brief but quite extreme climate cooling in the Northern Hemisphere. Fortunately, the Gulf Stream would eventually speed up again for reasons that remain poorly understood. It is thought that the exchange of water between the Atlantic Ocean and the Mediterranean Sea through the Strait of Gibraltar plays an important role in bringing the Gulf Stream back to speed. In order to test this idea, we need to know the strength of the Atlantic-Mediterranean exchange during times at which the Gulf Stream slowed down. Little shell-like organisms called benthic foraminifera, which live at the bottom of the ocean, record information about the properties of the water in which they grow within their shells. By analyzing a set of foraminifera living at a location close to the Strait of Gibraltar, we infer that it is indeed likely that the Atlantic-Mediterranean exchange changed significantly during a slowdown of the Gulf Stream. It is questionable whether or not the Gibraltar exchange will also intensify due to the current melting of ice.

1. Introduction

The largest climatic oscillations of the past 20 kyr coincide with dramatic changes in the rate of the Atlantic Meridional Overturning Circulation (AMOC) and associated northward heat transport (McManus et al., 2004). These oscillations are distinctive features of late Pleistocene deglaciations and hence fundamental to understand future oceanographic changes resulting from the current melting of the Greenland ice sheet (Hu et al., 2009). To date, the physical processes that facilitate the transition from sluggish glacial to strong interglacial AMOC over late Pleistocene deglaciations remain poorly understood.

By effectively mixing of relative fresh North Atlantic Central Water (NACW) with dense Mediterranean Outflow Water (MOW), the Gibraltar exchange enhances buoyancy of North Atlantic surface waters (Bigg et al., 2003). In particular, penetration of MOW into the Nordic Seas under high-index conditions of the North Atlantic Oscillation transfers salt to key sites of North Atlantic Deep Water (NADW) formation,

promoting deep convection (Lozier & Stewart, 2008). Moreover, the remnant MOW that does not fully penetrate northward of the Greenland-Scotland ridge presumably participates in overturning to the west of Ireland, within the path of the North Atlantic Drift (McCartney & Mauritzen, 2001; New et al., 2001). Today, without the injection of MOW salt, the AMOC could slow down by approximately 15% (Price & Yang, 1998; Rahmstorf, 1998; Wu et al., 2007).

The strength, here defined as volume and density, and location of the MOW plume within the Gulf of Cadiz determine the depth in which the MOW plume progresses and admixes further into the Atlantic Ocean. They determine how much buoyancy exchange will take place among North Atlantic intermediate water masses and the MOW. The amount and location of this buoyancy exchange affects NADW formation through deep water convection in the North Atlantic. During the last deglaciation, a shoaling and relocation of the MOW plume within the Gulf of Cadiz could have provided an important preconditioning for the abrupt resumption of AMOC around 14.6 kyr before present (Ivanovic et al., 2014; Rogerson et al., 2006). Enhanced buoyancy exchange at Gibraltar during Atlantic freshening phases could have provided a strong negative feedback to reduced AMOC (Bigg & Wadley, 2001; Reid, 1979; Rogerson et al., 2010; Sánchez Goñi et al., 2016; Toucanne et al., 2007; Voelker et al., 2006). The strength and location of the MOW plume are expressed in the temperature and salinity depth profiles in the water of the Gulf of Cadiz. Therefore, accurate and high-resolution temperature and salinity reconstructions allow estimating past strength and location of MOW and its influence on deglacial deep ocean circulation (Rogerson et al., 2012).

MOW variability can be studied in the Gulf of Cadiz due to the development of an extensive contourite system through the direct influence of the MOW (Hernàndez-Molina et al., 2013). For this purpose, Integrated Ocean Drilling Program (IODP) Expedition 339 drilled several sites that are presently situated with the upper and lower core of the MOW. Here we combine the Mg/Ca-based (e.g., Lear, 2000; Nürnberg, 1995) and the clumped isotope-based (Ghosh et al., 2006) paleoseawater thermometers to reconstruct temperature and salinity of the MOW across the last deglaciation to disentangle how the MOW influences the AMOC. We present a record of variability in these conditions for the last 22 kyr at IODP Site U1390, approximately 1,000 m deep within the central Gulf of Cadiz. We show that the glacial Mediterranean Outflow was much saltier than today. Furthermore, we show that Mg/Ca-based temperature measurements in Mediterranean deep waters are only interpretable once they are combined with clumped isotope-based temperature measurements.

2. Modern Hydrographic Setting

MOW is a combination of Mediterranean Levantine Intermediate Water (LIW) and Western Mediterranean Deep Water (WMDW) (e.g., Millot et al., 2006) (Figure 1). Upon exiting the Strait of Gibraltar, MOW follows the shelf down slope through the Gulf of Cadiz and flows northwestward settling as an intermediate contour current in several layers within the North Atlantic. Its salinity from 36.5 to 37.5 and temperature from 10.5 to 14.0°C (Baringer & Price, 1997; Borenäs et al., 2002; Cabeçadas et al., 2002) are observed between 300 and 1,400 m depth (Ambar & Howe, 1979). Note that the temperature signature of MOW is less prominent than its salinity signature in the Gulf of Cadiz (Figure 1; Ambar et al., 2002; Borenäs et al., 2002; Cabeçadas et al., 2002).

While flowing northwestward, MOW admixes with, or entrains eastern NACW (eNACW) and NADW. Entrained eNACW has both subtropical and subpolar origins (eNACWst and eNACWsp). The eNACWst is formed along the Azores Front and advected to the Iberian margin between 100 and 250 m depth (Fiúza et al., 1998; Voelker et al., 2015). The eNACWsp is formed in the vicinity of the Rockall Plateau and hence encountered between 250 and 500 m depth along the western Iberian margin (Brambilla et al., 2008). Through entrainment and admixing, MOW transfers its salt to the subpolar and subtropical gyres (e.g., Reid, 1979; Voelker et al., 2015), which in turn participate in North Atlantic deep convection.

3. Material and Methods

3.1. Site Description and Sampling

We studied samples from all three holes at IODP Site U1390 (A, B, and C) (IODP Expedition 339, 36°19.110′N, 7°43.078′W; Figure 1) down to 21.23 m composite depth scale. Figures 1c–1e are purely illustrative as the

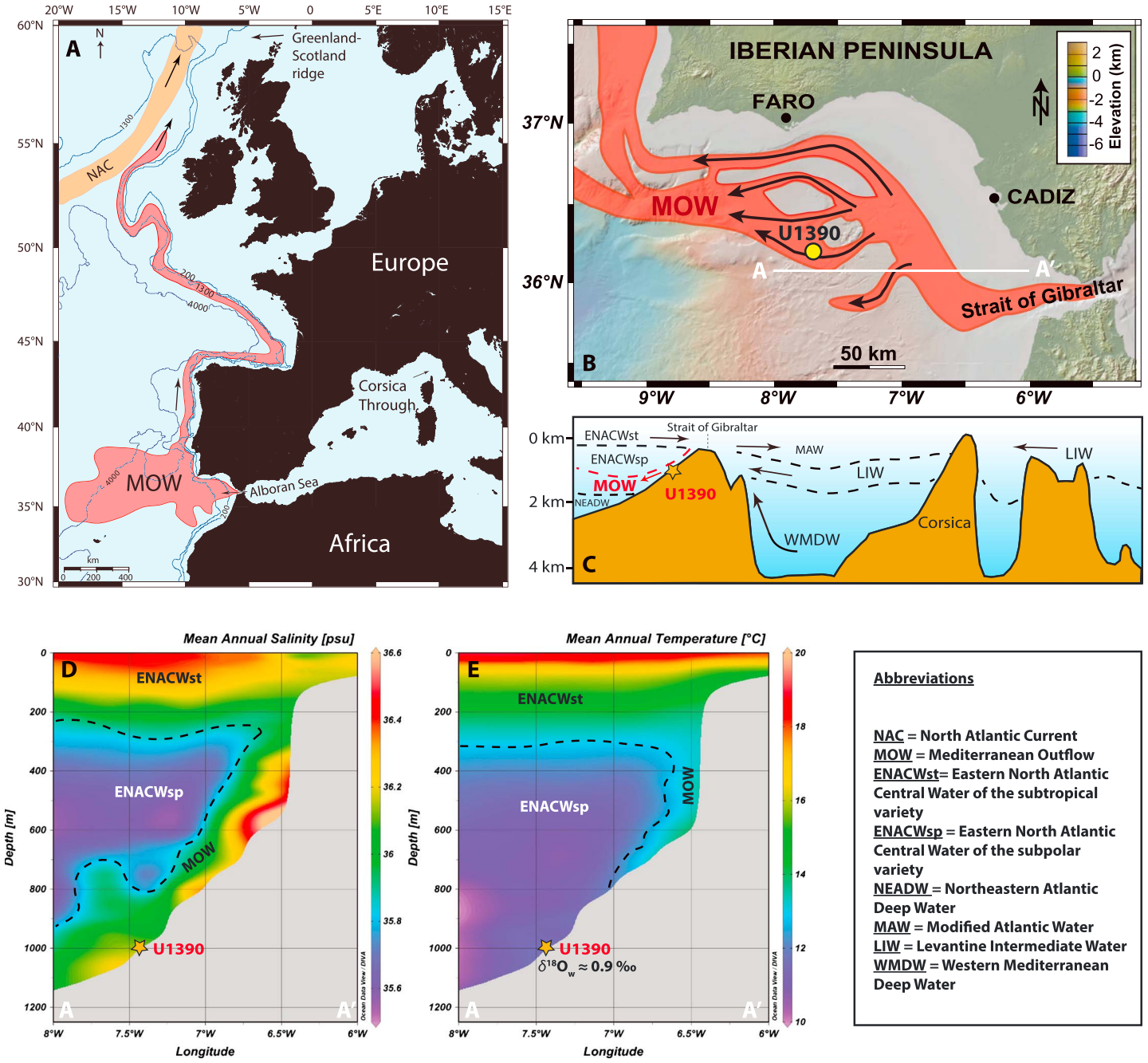

Figure 1. (a) The Mediterranean Outflow Water (MOW) plume as it progresses along the Iberian Margin toward the Greenland-Scotland Ridge (modified from Iorga & Lozier, 1999; Khélifi et al., 2009). (b) Location of Integrated Ocean Drilling Program 339 Site U1390 within the flow path of MOW (Bahr et al., 2015). The flow paths are based on Hernández-Molina et al. (2014). (c) A sketch of the water mass distribution in the Mediterranean Basin and in the Gulf of Cadiz with the location of Site U1390 projected on the sketched 2-D transect (modified from Cramp & O'Sullivan, 1999). Mean annual salinity and temperature profiles (d and e) from the World Ocean Atlas "13 database (averaged from 1955–2012 on a 0.25° resolution at 36.1°N; A-A" transect in Figure 1b (Locarnini et al., 2013; Zweng et al., 2013) made with Ocean Data View software (Schlitzer, 2017). Abbreviations of the water masses in the Gulf of Cadiz are based on Voelker et al. (2015). The core-top $\delta^{18}O_w$ (Figure 1e) is taken from Stow et al. (2013) (their Figure F34).

assigned locations of Site U1390 do not correspond to its exact coordinates. Site U1390 is characterized by high rates (>75 cm/kyr) of MOW contourite sedimentation without any hiatuses during the last deglaciation (Hernández-Molina et al., 2014) allowing reconstruction of millennial-scale fluctuations in temperature and salinity. Cores were sampled at 2 cm intervals, washed, sieved, and separated into <38,

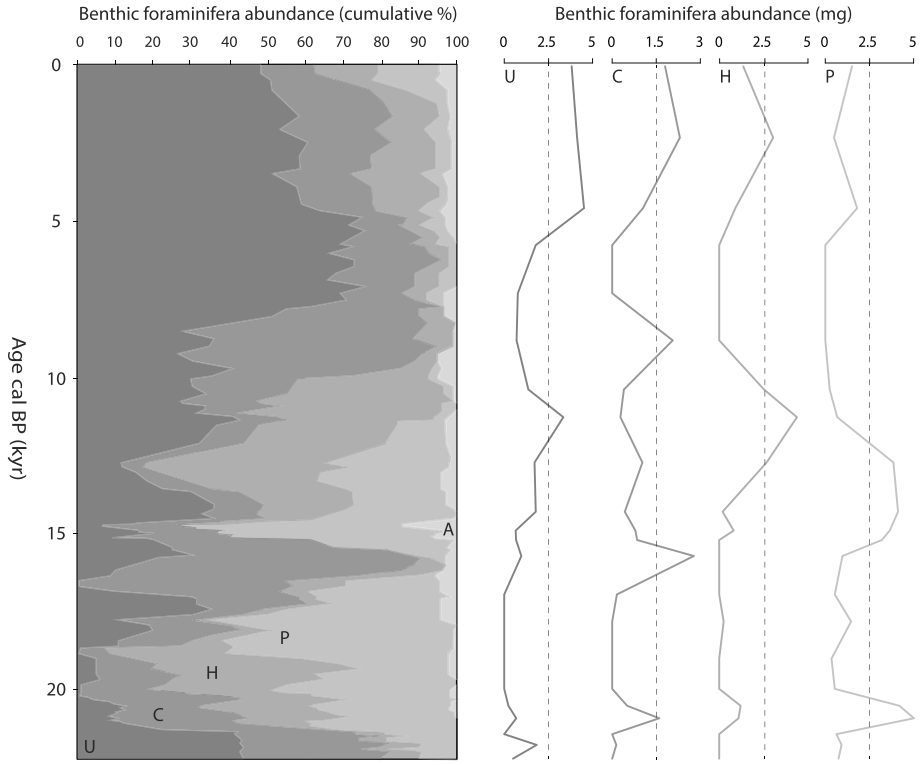

Figure 2. Specimen abundance (left: cumulative percentage of the total and right: absolute weight in mg) of the five most abundant benthic foraminifera (U = *U. mediterranea*, C = *C. pachyderma*, H = *H. elegans*, P = *Pyrgo spp.* and A = *P. ariminensis*) at Site U1390 across the last deglaciation.

63–150, and >150 μm fractions. Samples were dry-sieved to obtain the >212 μm fraction from which foraminifers were selected for analysis. For ^{14}C analysis, foraminifera were picked from the >150 μm fraction.

3.2. Stable Isotopes and Measurement Tactic

In order to perform stable isotope analysis, Mg/Ca-based thermometry and clumped isotope-based thermometry on benthic foraminifera, we analyzed most specimens present in the three cores. To plan the measurement strategy, we counted the most abundant species present in the cores (*Uvigerina mediterranea*, *Cibicidoides pachyderma*, *Hoeglundina elegans*, and *Pyrgo* spp.; Figure 2). Although *P. ariminensis* is also present at Site U1390, its abundance throughout the studied time interval is insufficient for the purpose of this study. As *U. mediterranea* was most abundant across most of the studied time interval, we determined δ^{18}O and δ^{13}C throughout the core for this species. Since *U. mediterranea* is a partially shallow infaunal species (0–1 cm; Fontanier et al., 2006), its carbon isotope signature does not necessarily reflect bottom water δ^{13}C. Hence, we produced another record of δ^{18}O and δ^{13}C using *C. pachyderma*. Although this species is not strictly epibenthic (Fontanier et al., 2006; Wefer & Mulitza, 2004), it has been used before to record changes in bottom water masses in the Gulf of Cadiz (e.g., Voelker et al., 2006). Most specimens of the four most abundant species were analyzed for Mg/Ca-based and clumped isotope-based thermometry to reconstruct past deep water temperatures (DWTs). As not all four species were equally abundant, we analyzed at least two species using the same method within every time interval. This allows us to evaluate potential interspecies differences in Mg/Ca and clumped isotope-based DWT. Note that we assume that there is no significant temperature difference between the pore water in the sediments in which the infaunal species dwell (e.g., *Pyrgo* spp. 0–3 cm depth; Linke & Lutze, 1993) and the waters present at the sediment surface, as has been shown before (Elderfield et al., 2010; Thornalley et al., 2015).

In order to construct an age model (see section 3.5), we measured the stable oxygen (and carbon) isotope composition on 15–30 specimens of the planktic foraminifera *G. bulloides* per sample. Specimens of *G. bulloides* and 1–5 specimens of *U. mediterranea* were analyzed (per sample) at Utrecht University. Crushed

specimens were washed with an ethanol solution in an ultrasonic bath to remove impurities and dried at 40°C overnight. Samples were dissolved in 104% phosphoric acid for 7 min at 70°C in a Kiel III (Thermo Fisher Scientific). The stable oxygen and carbon isotope composition of the produced CO_2 was measured in a Thermo-Finnigan MAT 253 at Utrecht University. Calibration to the international carbonate standard NBS-19 and in-house standard NAXOS show an analytical precision better than 0.05‰ and 0.08‰ for $\delta^{13}C$ and $\delta^{18}O$, respectively.

We analyzed 2–10 specimens of *C. pachyderma* per sample at ETH Zürich at 70°C in a Gas Bench II (Thermo Fisher Scientific) using the procedures outlined in Breitenbach and Bernasconi (2011). Reaction products were purified by gas chromatography, and the CO_2 was measured in continuous flow mode on a Delta V Plus mass spectrometer (Thermo Fisher Scientific). The ETH Gas Bench II system is calibrated with international carbonate standards NBS-19 and NBS-18, and routine analysis is standardized using both the in-house standard Isolab B (ETH-2) and powdered Carrara marble (MS2) revealing a precision better than 0.05 ‰ and 0.07 ‰ for $\delta^{13}C$ and $\delta^{18}O$, respectively. All oxygen isotopes are corrected for acid fractionation using the Kim et al. (2007) fractionation factor of 1.008714.

3.3. Mg/Ca Measurements

Mg/Ca ratios were determined on *U. mediterranea*, *C. pachyderma*, and *H. elegans*. Approximately 300 μg was collected per sample (1–5 specimens) from the dry-sieved >212 μm fraction. Measurements were performed in duplicate where enough material was available. Presence of inorganic overgrowth was evaluated using a scanning electron microscope. Shells can possess a Mn/Mg oxide-rich coating formed if Mn^{2+} has been mobilized during anoxic breakdown of organic matter deeper within the sediment column (Barker et al., 2003). The contribution of Mn^{2+} from coatings to the corresponding Mg/Ca ratio is approximately 1% (Barker et al., 2003). To remove coatings, samples were gently crushed between two glass plates and cleaned according to the Cambridge protocol without the reductive cleaning step (Barker et al., 2003). Clay particles were removed by repeated rinses with Milli-Q. Organic matter was subsequently removed by subboiling of the samples twice in alkali buffered 1% H_2O_2 for 10 min. Samples were then transferred onto a glass plate under a microscope for visual removal of coarse-grained silicates. Then, samples were briefly acid-leached in 0.001 M HNO_3 after which the samples were dissolved in 0.075 M HNO_3. The final solutions were analyzed on an Element2 Inductively Coupled Plasma mass spectrometer (Thermo Scientific) after dilution to a 20 parts per million (ppm) Ca matrix to maximize accuracy of elemental ratios. Accuracies were determined using the JCp-1 *Porites* spp. (Okai et al., 2001) coral standard and was 99.3% (4.17 mmol/mol) for Mg/Ca. Accuracy was improved using drift corrections with an in-house coral monitor standard. Short-term (<5 min) precision was typically 0.3% for Mg/Ca. Short-term precision reflects variability in operating conditions such as power and gas flow rates. Longer-term stability mainly reflects the goodness of drift corrections. Blanks were kept low using ultrapure acids and were always <0.5%. Possibly contaminated specimens were rejected based on examination of Fe/Ca, Al/Ca, and Mn/Ca concentrations (Barker et al., 2003; see section 4.2) along with specimens showing signs of dissolution and/or overgrowth. Most of the foraminifera were glassy and showed no signs of overgrowth or dissolution. We argue that preservation of the foraminifera was optimal in the sandy contourite sediments, which quickly covered the specimens under the high sedimentation rate at Site U1390 (>75 cm/kyr).

Mg/Ca ratios were translated to DWT using the equations reported below for *Cibicides* spp., *Uvigerina* spp., and *H. elegans*, respectively. Out of all published calibrations, these provide the most accurate DWTs with respect to the modern DWT at Site U1390. As we did not perform reductive cleaning, we corrected all Mg/Ca measurements on *C. pachyderma* and *H. elegans* down by 15% to be able to use the respective calibrations (Barker et al., 2003). As the analytical error on the Mg/Ca ratios is relatively low and the resulting error on the formation temperature depends on the amount of Mg/Ca within the foraminifera, we base our error margins on the average standard deviation in formation temperature of duplicate measurements of the same foraminifera. The resulting error margins are 1.1°C for *U. mediterranea*, 0.8°C for *C. pachyderma*, and 0.6°C for *H. elegans* (supporting information). Note that these uncertainties do not include the calibration error.

$$\mathrm{Mg/Ca} = 0.90(\pm 0.037)\exp 0.11(\pm 0.003)T(°\mathrm{C}) \quad (\textit{Cibicides}\ \text{spp.};\ \text{Elderfield et al., 2006})$$

$$\mathrm{Mg/Ca} = 0.94(\pm 0.044)\exp 0.053(\pm 0.004)T(°\mathrm{C}) \quad (\textit{Uvigerina}\ \text{spp.};\ \text{Elderfield et al., 2006})$$

Table 1
Age Constraints Used to Derive the Age Model

Age model					
mcd (m)	AMS labcode	Age cal BP (Calib 7.0.4)	2 sigma (Calib 7.0.4.)	Stratigraphic tie point (Steffensen et al., 2008)	Sedimentation rate (m/kyr)
0.10	SacA33890	219	94–306	—	0.79
0.39	UCI122484	588	538–634	—	0.38
1.76	SacA33892	4197	4,085–4,299	—	0.75
4.52	SacA33893	7,890	7,813–7,957	—	0.67
5.96	SacA33894	10,040	9,902–10,154	—	0.79
6.64	—	—	—	10,850 (sharp negative excursion, cooling?)	2.00
6.80	—	—	—	10,930 (sharp negative excursion, cooling?)	1.40
7.07	UCI122485	11,167	11,086–11,239	—	3.14
7.76	SacA33896	11,393	1,1218–11,677	—	0.08
7.82	—	—	—	12,130 (YD)	0.73
8.14	—	—	—	12,570(YD)	0.50
8.30	—	—	—	12,890 (start YD)	0.61
8.95	—	—	—	13,950 (end BA)	1.07
9.59	—	—	—	14,550 (start BA)	3.46
11.95	—	—	—	15,230 (end HS1)	0.65
12.48	—	—	—	16,050 (start HS1)	0.95
16.30	SacA33889	20,136	19,727–20,518	—	2.36
21.09	SacA33890	22,169	21,920–22,376	—	0.95

Note. The uncertainty on the ^{14}C dates are mostly composed of the uncertainty on the calibration step.

$$\mathrm{Mg/Ca} = 0.4(\pm 0.18)\exp 0.16(\pm 0.02)T(^{\circ}\mathrm{C}) \qquad (H.\ elegans;\ \text{Lo Giudice Cappelli et al.}, 2015)$$

3.4. Clumped Isotope Measurements

The enrichment in clumped isotopologues defined as Δ_{47} was measured using an automated method for small carbonate samples (Meckler et al., 2014). To reach an adequate precision of 5 to 10 ppm in Δ_{47}, representing ±2°C in temperature space, about 30 measurements of ±150 μg calcite are required (Meckler et al., 2014). Hence, we measured 37 aliquots (18x *U. mediterranea*, 19x *Pyrgo* spp.) within the last glacial (20.9–21.9 ka), 38 aliquots (all *Pyrgo* spp.) within Heinrich Stadial 1 (HS1), and 36 aliquots (20x *U. mediterranea*, 10x *C. pachyderma* and 6x *Pyrgo* spp.) within the Holocene (1.2–3.5 ka).

Note that we measured only 8 aliquots between 10.3 and 11.4 ka. We include this measurement in this study because the standard deviation is exceptionally low (30 ppm). One typically reaches such a standard deviation, corresponding to a standard error of 5 to 10 ppm, only after 20–30 measurements. Nevertheless, as in this case the standard error does not always capture the 95% confidence interval (Fernandez et al., 2018) we here doubled the error margin to 5.6°C (Table 2).

Measurements were performed using a Thermo Scientific Kiel IV carbonate device coupled to a Thermo Scientific MAT 253 isotope ratio mass spectrometer at the ETH Zürich modified with a Porapak® trap to remove unidentified organic contaminants that can create isobaric interferences during clumped isotope measurements. The used correction scheme is described by Meckler et al. (2014). All Δ_{47} measurements were converted to the absolute reference frame (Dennis et al., 2011) and corrected for an acid digestion of 70°C (Henkes et al., 2013). Temperatures were estimated using the following calibration equation (Kele et al., 2015):

$$\Delta_{47} = \frac{0.04371 \times 10^6}{T(^{\circ}\mathrm{K})^2} + 0.205S.$$

We assume that there are no significant temperature variations within the four time intervals used to calculate an average Δ_{47} by pooling adjacent samples as suggested by Grauel et al. (2013). This assumption is presumably valid for intervals with a constant $\delta^{18}O_c$ of *U. mediterranea*, as variations in temperature and/or salinity will result in variations in $\delta^{18}O_c$. We measured multiple aliquots of each species separately and only pooled all aliquots to average temperatures during the postprocessing phase.

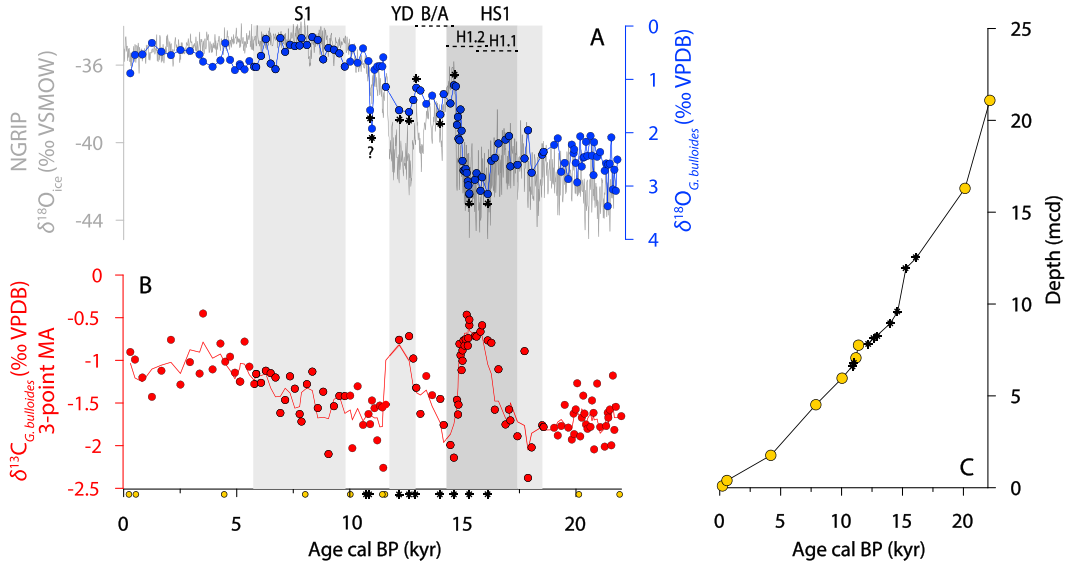

Figure 3. (a) Planktic $\delta^{18}O$ (*G. bulloides*) tuned to the NGRIP $\delta^{18}O_{ice}$ deglacial age scale (Steffensen et al., 2008) based on nine visual stratigraphic tie points (black marks) and nine ^{14}C dates (yellow circles) (Table 1). (b) Planktic $\delta^{13}C$ (*G. bulloides*) recording two positive excursions during HS1 and YD. (c) Age model (meters composite depth (mcd) scale) at Site U1390 (Table 1) with the yellow circles and black marks representing the visual tie points and ^{14}C dates, respectively. Age ranges: S1; 9.8–5.7 kyr cal BP (De Lange et al., 2008), YD; 12.7–11.7 kyr cal BP, Bølling-Allerød (B/A); 14.7–12.9 kyr cal BP (Steffensen et al., 2008) and HS1; 18–14.3 kyr cal BP with H1.1; 17.1–15.5 kyr cal BP and H1.2; 15.9–14.3 kyr cal BP (Hodell et al., 2017).

3.5. Age Model

Nine samples of bulk planktonic foraminifera (after removing *Globorotalia* spp. and *G. calida*) were used for ^{14}C dating (Table 1 and Figure 3). Samples were treated in 2 mL of 0.01 M nitric acid for 15 min to remove organic coatings. Subsequently, samples were dried under vacuum and dissolved in phosphoric acid at 60°C to produce 1 mg of carbon as CO_2. The CO_2 was reduced with H_2 in presence of iron at 600°C to graphite and pressed directly onto a target. The activity of ^{14}C in the graphite targets was measured on an Advanced Relay And Technology Mission (ARTEMIS) mass spectrometer and standardized using in-house CO_2 standard HOxI that was normalized to a $\delta^{13}C$ value of -25‰. ^{14}C activity was corrected for fractionation in the mass spectrometer based on the $\delta^{13}C$ measurement. Radiocarbon age was calculated after Mook and van der Plicht (1999). Radiocarbon ages were calibrated to calendar years before present (age cal BP) using Calib 7.0.4 (Stuiver et al., 2017) and MARINE13 (Reimer et al., 2013).

As large changes in reservoir age are likely to occur throughout the deglaciation, we corrected for these changes using stratigraphic tie points based on the visual correlation between the planktonic $\delta^{18}O$ (*G. bulloides*) and the North Greenland Ice Core Project (NGRIP) deglacial age scale (Steffensen et al., 2008), which was converted into BP ages by subtracting 50 years (Table 1) to complete the age model (Figure 3). Visual correlations are based on the timing of the HS1 (Hodell et al., 2017), the Younger Dryas (YD), and the Bølling-Allerød (B/A) interstadial as defined in the NGRIP record (Steffensen et al., 2008) (Table 1 and Figure 3). Note that we visually correlated the sharp decrease in $\delta^{18}O_{planktic}$ of approximately 1‰ from 6.6 to 6.8 m composite depth scale to a small decrease in the NGRIP record at 10 kyr as the decrease occurs too late to correspond to the YD (Table 1 and Figure 3).

3.6. Grain Size Analysis

Grain size analysis was performed by analyzing the untreated weights of the washed $<$38, 63–150, and $>$150 μm fractions. Specifically, the coarser fraction between 63 and 150 μm should decrease during times of reduced MOW strength. By excluding grain sizes above 150 μm, we remove a significant part of the carbonate biomass endmember within the contourite sediments (Rogerson et al., 2005).

3.7. Reconstruction of Relative Salinity Changes

In order to convert $\delta^{18}O_c$ into salinity (supporting information), we first estimate Late Holocene ($<$5 kyr) $\delta^{18}O_{water\ (w)}$ using an *Uvigerina* spp. calcite-water oxygen isotope fractionation calibration from 4 to 18°C

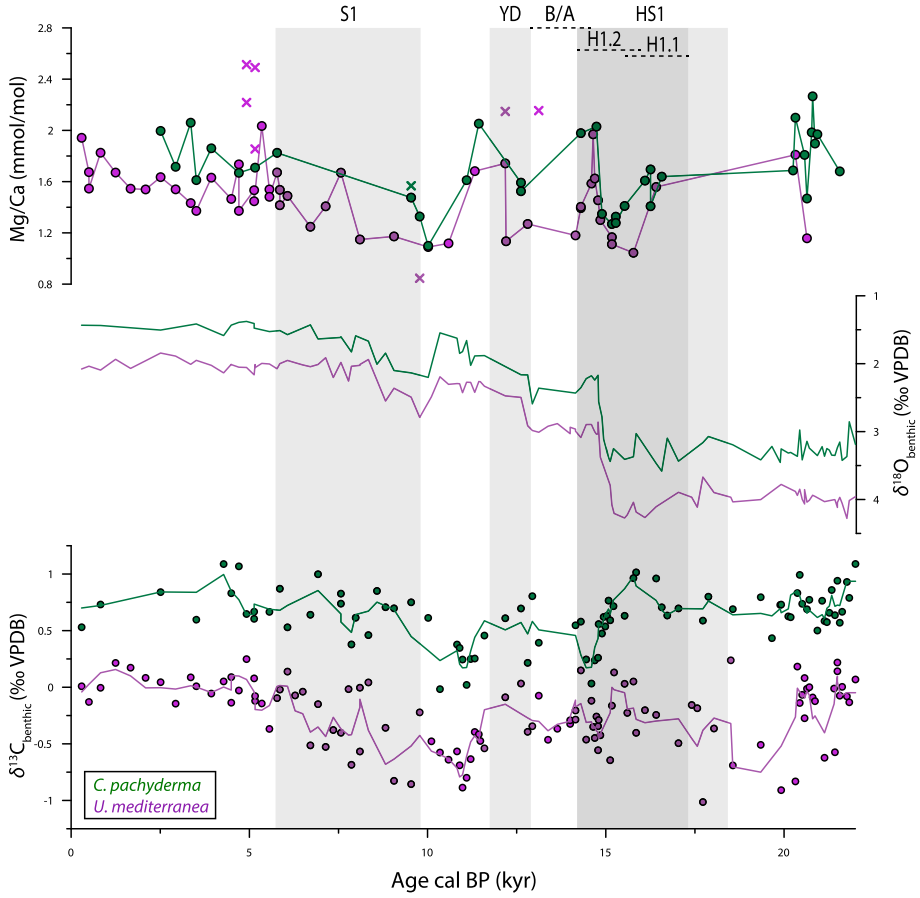

Figure 4. $\delta^{18}O$, $\delta^{13}C$, and Mg/Ca records of *U. mediterranea* (purple) and *C. pachyderma* (green).

(Marchitto et al., 2014). Here we insert the $\delta^{18}O_{calcite\ (c)}$ of *U. mediterranea* and either the reconstructed DWT based on the Mg/Ca of *U. mediterranea* or the record of clumped isotope-based DWT. For this calculation we averaged duplicate Mg/Ca-based DWTs and excluded several outliers (see section 4.2). The Marchitto et al. (2014) regression is valid since the estimated Late Holocene $\delta^{18}O_w$ is within uncertainty of the measured core-top $\delta^{18}O_w$ (Stow et al., 2013; 0.9‰, Figure 1). Subsequently, we normalize the down-core estimates of $\delta^{18}O_w$ to the Late Holocene $\delta^{18}O_w$. Then, we correct the $\delta^{18}O_w$ anomalies relative to the Late Holocene for the global change in $\delta^{18}O_w$ over the deglaciation, producing a record of $\delta^{18}O_{w\text{-}ivf}$ (Austermann et al., 2013; Waelbroeck et al., 2002).

A comprehensive survey of modern surface waters shows a linear correspondence between salinity and $\delta^{18}O_w$ and suggests a slope of 0.27 ‰ $\delta^{18}O_w$/salinity for Mediterranean waters (Pierre, 1999). This relationship is likely representative for the Last Glacial Maximum (LGM), as the endmembers providing fresh water to the Mediterranean did not change significantly (Rohling, 1999). Nevertheless, the slope of the $\delta^{18}O_w$/salinity relationship in the North Atlantic might have been significantly steeper during the LGM (Holloway et al., 2015; Legrande & Schmidt, 2011; Rohling, 2007) and during the YD (Lynch-Stieglitz et al., 2011) due to pronounced changes in the freshwater endmembers. Similarly, the slope of the $\delta^{18}O_w$/salinity relationship in the Mediterranean might have been twice as steep at 7/8 ka under the intensified monsoon circulation resulting in the deposition of Sapropel 1 (S1) (Rohling & De Rijk, 1999). Hence, we extrapolate both the modern (0.27) and a twice as steep (0.52) $\delta^{18}O_w$/salinity relationship over the deglaciation.

4. Results

4.1. Stable Isotope and Grain Size Measurements

Planktic $\delta^{18}O$ decreases by approximately 2.5 ‰ over the deglaciation and is at a maximum during the final stage of HS1 (Figure 3). Planktic $\delta^{13}C$ shows two positive excursions during HS1 and YD after which it

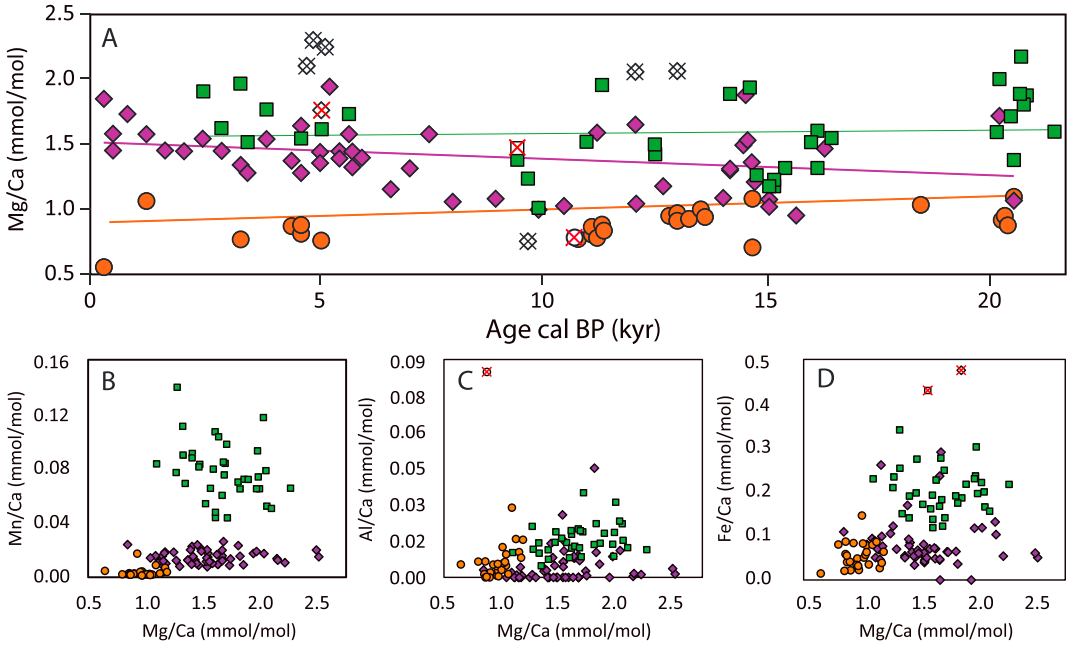

Figure 5. (a) Foraminiferal Mg/Ca indicating no significant trends in Mg/Ca across the last deglaciation. (b) Mn/Ca versus Mg/Ca for *U. mediterranea* (purple), *C. pachyderma* (green), and *H. elegans* (orange). (c) Al/Ca versus Mg/Ca. (d) Fe/Ca versus Mg/Ca. Outliers are indicated with crosses (see section 4.2). Red crossed samples are excluded based on relatively elevated Mn/Ca, Al/Ca, and/ or Fe/Ca ratios. Black crossed samples are excluded because they represent unrealistically high or low deep water temperatures.

gradually increases by 1‰ toward the Holocene. Benthic δ^{18}O shows a similar decrease of approximately 1.5‰ during HS1 and 0.5‰ during the YD (Figures 4 and 6). Furthermore, we find a brief positive excursion of approximately 0.5 ‰ at the start of S1 (as defined in De Lange et al., 2008). Benthic δ^{13}C decreases by 0.4‰ during the later phase of HS1 and remains relatively low until the start of S1. Although the benthic δ^{13}C of *C. pachyderma* is on average 0.5‰ more enriched than the δ^{13}C of *U. mediterranea*, the relative changes are indifferent (Figure 4). In line with previous studies, benthic δ^{18}O of *C. pachyderma* is approximately 0.5‰ more depleted than the δ^{18}O of *U. mediterranea* (Shackleton, 1974; Voelker et al., 2006) (Figure 4). The abundance of grain sizes between 63 and 150 μm is greatest during the LGM and decreases at the start of H1.1 (Figure 6f). After a brief and rapid positive excursion during H1.2, the grain size fraction is relatively coarse until the end of the YD. Then, the fraction decreases gradually toward S1 where it drops to a minimum. The coarse grain size fraction gradually increases again after S1 but does not reach the relatively heavy LGM weights.

4.2. Trace Elemental Ratios, DWT Estimates and Relative Salinity Reconstruction

Mg/Ca in *U. mediterranea*, *C. pachyderma*, and *H. elegans* vary between 0.8 and 2.5, 1.10 and 2.27, and 0.65 and 1.19 mmol/mol, respectively. There is no significant difference in benthic foraminiferal Mg/Ca between glacial and interglacial samples (Figure 5). The Mg/Ca records of *C. pachyderma* and *U. mediterranea* are very similar (Figures 4 and 5). Although we find no species-specific correlations between Mg/Ca and Mn/Ca, Al/Ca, or Fe/Ca, we excluded three samples with relatively elevated Al/Ca and Fe/Ca ratios (Figure 5).

Temperature reconstructions based on the epibenthic foraminifers *C. pachyderma* and *H. elegans* indicate an average Holocene DWT of 4.5 ± 1°C in the Gulf of Cadiz (Figure 6a). Reconstructions based on the shallow infaunal species *U. mediterranea* are in good agreement with the present-day DWT (Figure 6a). Apart from the Mg/Ca measurements neglected based on the Mn/Ca, Al/Ca, and Fe/Ca ratios, we excluded six more Mg/Ca measurements (Figure 5) on *U. mediterranea* because they exceed the expected DWT range at Site U1390 between 0 and 15°C (Figure 1). We argue that the exceedingly high Mg/Ca in some of the samples is related to downslope transport of single specimens of *U. mediterranea* that lived in shallower and warmer waters along the shelve.

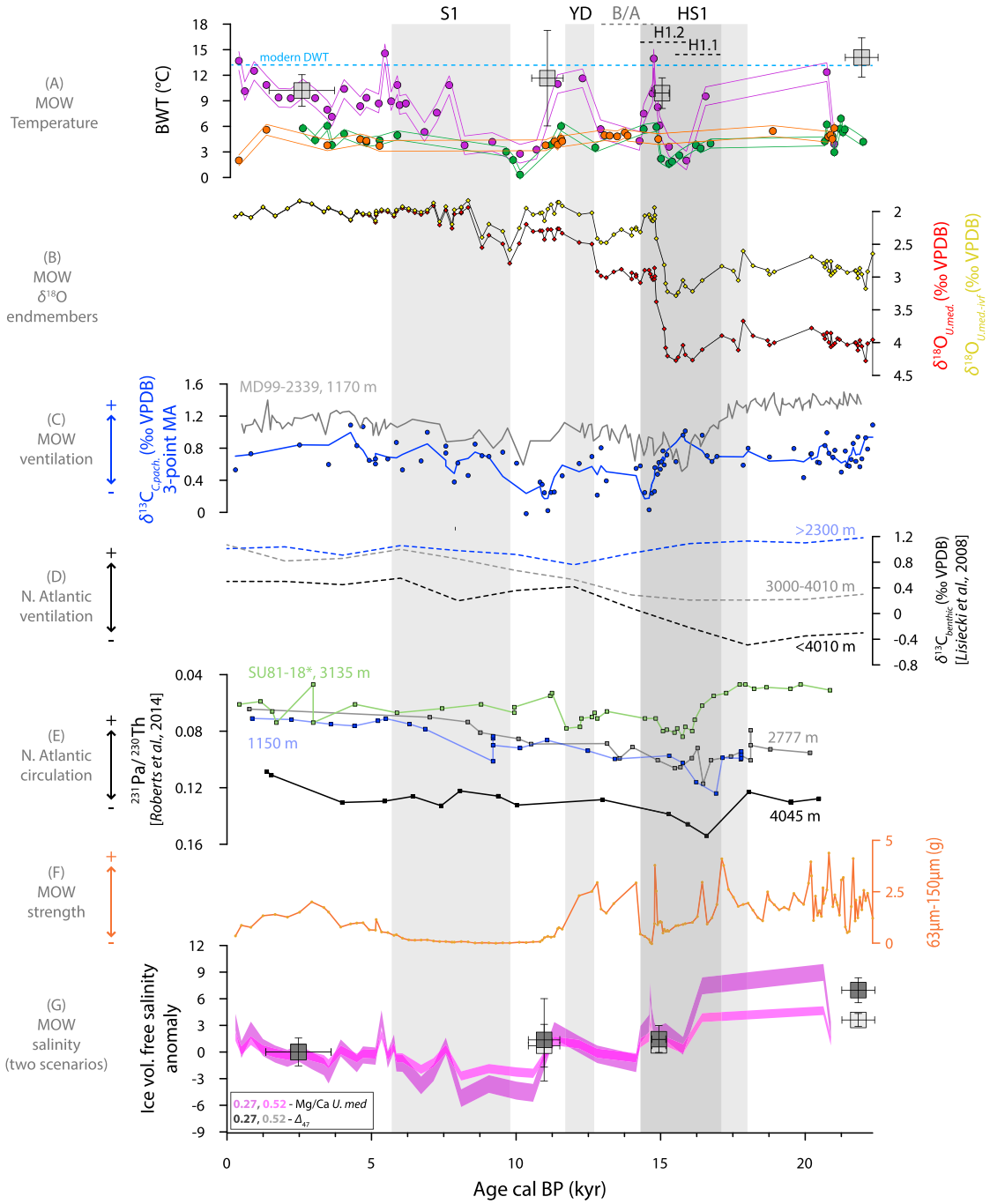

Figure 6. Temperature and salinity reconstruction of Mediterranean Outflow Water (MOW) across the last deglaciation (0–22 ka). (a) Deep water temperature (DWT) based on Mg/Ca-thermometry (circles) derived from epibenthic to shallow infaunal *C. pachyderma* (green), epibenthic *H. elegans* (orange), and shallow infaunal *U. mediterranea* (purple); DWT based on pooled Δ_{47} measurements of different benthic species (Table 2). Horizontal error margins depict the age spread of the pooled measurements (Table 2). Vertical error margins represent mainly the analytical error and the external reproducibility of the measurements (see section 3). The thin dashed lines mark the present DWT of 13.1°C (Stow et al., 2013). Possible intrusions of NEADW at Site U1390 are marked with the black arrows. (b) Evolution of different oxygen isotope endmembers across the last deglaciation; $\delta^{18}O$ (‰ Vienna Pee Dee Belemnite (VPDB)) of *U. mediterranea* (red diamonds) corrected for ice volume change (yellow diamonds). (c) MOW ventilation as recorded by the $\delta^{13}C$ (‰ VPDB) of *C. pachyderma* documenting two significant negative excursions during H1.2 and before the start of S1 at Site U1390 (blue) and Site MD99-2339 (gray; Voelker et al., 2006). (d) North Atlantic ventilation as recorded in the $\delta^{13}C$ of North Atlantic waters at different depth intervals (Lisiecki et al., 2008). (e) North Atlantic circulation strength recorded by Pa/Th data (Gherardi et al., 2005; Roberts et al., 2014). (f) MOW strength as recorded by the coarse grain size fraction between 63 and 150 µm. (g) MOW salinity estimated using two oxygen isotope endmember scenarios (see section 3) recording two significant decreases in salinity during HS1 and S1. The purple and gray colors represent the salinity reconstructions using the Mg/Ca-based DWT of *U. mediterranea* and the clumped isotope-based DWT, respectively. The lighter colors represent the 0.52 $\delta^{18}O_w$/S endmember scenario.

Table 2
Clumped Isotope Measurements and Respective Temperatures

Clumped isotope-based BWT at Site U1390 based on three species of benthic foraminifera					
Age cal BP	*U. mediterranea*	*Pyrgo* spp.	*C. pachyderma*	Pooled	BWT (°C)
1.2–3.5 kyr	0.751 ± 0.037 (20)	0.748 ± 0.065 (6)	0.748 ± 0.045 (10)	0.749 ± 0.007 (36)	10.2 ± 1.8
10.3–11.4 kyr	0.744 ± 0.010 (8)	—	—	0.744 ± 0.022 (**8**)[a]	11.7 ± **5.6**
14.7–15.2 kyr	—	0.750 ± 0.045 (38)	—	0.750 ± 0.007 (38)	9.6 ± 1.8
21.2–22.3 kyr	0.737 ± 0.044 (18)	0.733 ± 0.033 (19)	—	0.735 ± 0.006 (37)	14.2 ± 1.7

Note. The numbers of aliquots measured are indicated in between the brackets.
[a]For the pooled aliquots (see section 3.4) between 10.3 and 11.4 kyr we doubled the uncertainty to accurately reflect the 95% confidence interval (Fernandez et al., 2018).

All three Mg/Ca-based DWT records suggest no difference in DWT between the LGM and the Holocene. Furthermore, the Mg/Ca-based DWT records of *C. pachyderma* and *U. mediterranea* indicate several temperature minima, which are more pronounced in the record of *U. mediterranea*. Specifically, the *U. mediterranea* record suggests a cooling of approximately 7°C at the start of H1.2, at the end of H1.2 and just before the start of S1.

Pooled Δ_{47} measurements of three species also suggest no difference in DWT between the LGM and the Holocene, although a slight cooling cannot be disregarded entirely (Table 1 and Figure 6a). Furthermore, we observe no difference in the clumped isotope-based DWT reconstructions among the three benthic species (Table 2 and Figure 4).

As the absolute Mg/Ca-based DWTs on *C. pachyderma* and *H. elegans* are colder than modern-day DWT, we considered only the *U. mediterranea* Mg/Ca-based DWT and the four clumped isotope-based DWT reliable to estimate salinity changes at Site U1390. Considering both records of DWT, we infer a salinity decrease of MOW by three to eight units from the LGM to the Holocene over the deglaciation accounting for the global ^{18}O depletion due to decreasing Northern Hemisphere glaciation. We find another significant salinity decrease of approximately four units during S1.

5. Discussion

5.1. Nontemperature Effects on Benthic Mg/Ca

Mg/Ca-based DWT on the epibenthic foraminifers *C. pachyderma* and *H. elegans* are significantly lower than the present-day annual DWT at the Site (13.1°C, Stow et al., 2013). A similar offset between Mg/Ca-based and core-top DWT is reported for *C. pachyderma* in the Alboran Sea (Cacho et al., 2006). This discrepancy cannot be explained by altered Mg/Ca due to postmortem dissolution as MOW at Site U1390 is highly supersaturated with respect to calcite ($\Delta[CO_3^{2-}] > 70$ μmol kg^{-1}; Aït-Ameur & Goyet, 2006; Key et al., 2015). The high alkalinity would rather induce postmortem Mg-rich overgrowths on the foraminiferal tests (Groeneveld et al., 2008) and result in an overestimation of DWT, which is unlikely with the relatively low DWTs reported here. Theoretically, high MOW salinity would be expected to also increase foraminiferal Mg/Ca (Lea et al., 1999; Nürnberg et al., 1996). Some culture and core-top evidence exists for a reduction in Mg incorporation in waters highly oversaturated in carbonate ion concentration (Lo Giudice Cappelli et al., 2015; Russell et al., 2004). However, other studies indicate that the impact of saturation state on Mg-incorporation is very small or absent (Dueñas-Bohórquez et al., 2009, 2011; Raitzsch et al., 2008). This discrepancy is presumably related to interspecies geochemical differences or by variability in the applied culture conditions in comparison to the environmental conditions.

Reconstructions based on the shallow infaunal species *U. mediterranea* are in good agreement with the present-day DWT (Figure 6a). Interestingly, the Mg/Ca records show a remarkable similarity between *C. pachyderma* and *U. mediterranea* (Figure 5). This similarity suggests a similar temperature dependency for both calcitic species in the MOW. To test this hypothesis, we need a specific calibration derived using core-top and culture data under high alkaline and saline conditions that also considers the data set of Cacho et al. (2006) in the Alboran Sea. Until then, we argue that it is debatable whether or not a positive correction to the intercept of the Mg/Ca calibration of *C. pachyderma* to fit the modern DWT of MOW, as

performed by Cacho et al. (2006), is justified. Besides the fact that a one-point core-top calibration can be inaccurate, performing such a correction will also give the impression that we have tackled the problems of Mg/Ca-thermometry in the high saline and high alkaline waters of the Mediterranean Sea. In fact, we might be dealing with a site-specific vital effect, possibly related to the high alkalinity of the Mediterranean waters, which does change not only the intercept of the applied open-ocean Mg/Ca calibration but also the temperature sensitivity. In addition, applying a correction to *C. pachyderma* will suggest that *H. elegans* is the only benthic species within our data set that is not fit for Mg/Ca thermometry in the Mediterranean Sea. In any case, a correction to the Mg/Ca-T calibration of *C. pachyderma* would not change the interpretations of this study. Mg/Ca-based DWTs on both epibenthic species would still indicate a constant LGM to Holocene DWT with slight drops in DWT, which are also recorded by *U. mediterranea* (Figure 6a). Our data set clearly demonstrates that Mg/Ca in benthic foraminifera is complicated in Mediterranean deep waters as observed before by Cacho et al. (2006). Hence, an alternative paleoseawater thermometer is needed.

5.2. Clumped Isotope-Based DWT and Synthesis

In contrast to the Mg/Ca-based DWT measurements, our clumped isotope-based DWT measurements confirm that there are no species-specific vital effects in benthic foraminifera that affect the clumped isotope composition of their tests (Tripati et al., 2010). Furthermore, Late Holocene DWT at Site U1390 is slightly cooler than the modern DWT but agrees well with the Mg/Ca-based DWTs of *U. mediterranea* within the respective time period (Figure 6a). The accuracy of the clumped isotope-based DWTs is inherent to the assumption that DWT does not change significantly within the averaged depth/time intervals. This assumption is presumably valid for the LGM, the Late Holocene and at 10.9 ka, when the respective $\delta^{18}O_c$ record no significant variability. In these intervals, the grain size ratio is also constant, suggesting that there is no significant change in the strength of the MOW plume and hence no variations in the temperature and salinity of the bottom waters (Figure 3). However, during H1.2, $\delta^{18}O_c$ decreases significantly (Figure 4). Nevertheless, as we observe no trend in Δ_{47} within the pooled 200 years' time interval (supporting information), the expected uncertainty in DWT is presumably within error of the clumped isotope measurement. In summary, both Mg/Ca (*of U. mediterranea*) and clumped isotope-based temperature estimates represent accurate reconstructions of MOW DWT at Site U1390. The combined records suggest no significant difference in DWT between the LGM and the Holocene although a slight cooling cannot be disregarded entirely. Furthermore, we find three significant drops in DWT at the start of H1.2, at the end of H1.2, and just before the start of S1.

5.3. A Stronger MOW at Site U1390 During the LGM

At present, Site U1390 is under the direct influence of MOW-induced contourite sedimentation (Faugères et al., 1984; Habgood et al., 2003; Hernández-Molina et al., 2014; Figure 1) being at the mouth of the Guadalquivir contourite channel (Stow et al., 2013). The calculated sedimentation rates are quite variable over the deglaciation with maxima reaching over 3 m/kyr (Table 1). Our age model does not have the precision required to resolve such drastic changes in sedimentation rates on submillennial time scales. Nevertheless, the average sedimentation rate increases toward the LGM together with an increase in the coarse grain size fraction (Table 1 and Figure 6f). Both parameters indicate the presence of a stronger MOW at Site U1390 during the LGM. This is further evidenced by the increase in MOW salinity and thus density toward the LGM (Figure 6g). The stronger presence of MOW during the LGM is also supported by a significant shift in the benthic foraminiferal community (Figure 2). According to the TROX model, deep infaunal foraminifera species like *Pyrgo* spp. are more likely found in bottom waters that are more anoxic (Jorissen et al., 1995). A stronger MOW during the LGM, being a water mass relatively poor in oxygen (e.g., Ambar et al., 2002; Cabeçadas et al., 2002), supports the observed shift in the benthic community.

Increased contourite sedimentation has also been documented at other sites within the central Gulf of Cadiz (Bahr et al., 2015; Llave et al., 2006; Rogerson et al., 2005; Schönfeld & Zahn, 2000). Thus, although there is a need for caution when interpreting the millennial-scale fluctuations presented in this study, our record confirms the presence of a stronger MOW at Site U1390 during the LGM.

5.4. Saltier Glacial Mediterranean Outflow

Increased MOW salinity during the LGM aligns well with known changes in Mediterranean circulation patterns over glacial-interglacial timescales. Due to a reduction in sill depth of the Strait of Gibraltar from 285 to 165 m during the LGM (Fairbanks, 1989), inflow and outflow volumes were reduced, and the impact of

the Mediterranean negative hydrologic budget on salinity was amplified by a longer residence time of Mediterranean waters (Matthiesen & Haines, 2003; Rogerson et al., 2010; Rohling, 1999). Specifically, the $\delta^{18}O_{w\text{-}ivf}$ of WMDW in the Alboran Sea (Figure 1) was 0.2 to 1‰ more enriched during the LGM than during the Holocene, reflected by pore water $\delta^{18}O$ measurements (Paul et al., 2001) and benthic $\delta^{18}O$ measurements (Cacho et al., 2006), respectively. Here we show that the change in $\delta^{18}O_{w\text{-}ivf}$ from LGM to Holocene was 1.5–2‰, which is greater than these previous estimates.

Nevertheless, modern MOW consists mostly of eastern Mediterranean Sea-derived water masses like the LIW (Millot et al., 2006) (Figure 1). In this view, the reported 2‰ increase in $\delta^{18}O_{w\text{-}ivf}$ of LIW through the Corsica Trough with respect to the Holocene (Toucanne et al., 2012) could explain the entire salinity anomaly reported here. However, over the deglaciation MOW might have been sourced by varying fluxes of LIW and WMDW (Jiménez-Espejo et al., 2015; Millot et al., 2006; Voelker et al., 2006).

Varying box models of the Mediterranean Sea estimate an increase in salinity of up to four units (1 ‰ in $\delta^{18}O_{w\text{-}ivf}$) compared to the Holocene (Bigg, 1995; Matthiesen & Haines, 2003; Myers et al., 1998; Rohling, 1999). But, if relative humidity, defined as the sea-air temperature difference, in fact, reduced from 0.8 in the Holocene to 0.6 in the LGM, the salinity anomaly would have been larger in the model simulations (Rohling, 1999). A reduced humidity during the LGM is supported by annual precipitation estimates from pollen analysis of marine core MD95-2043 retrieved in the Alboran Sea showing an increase of 400 mm in annual precipitation toward the Holocene (Fletcher et al., 2009). Thus, although the accumulation of salt in the Mediterranean Sea during the glacial low stand presumably resulted in a saltier MOW, it is not certain that the increase in Mediterranean Sea salinity explains the entire salinity anomaly of MOW presented here.

5.5. Atlantic-Mediterranean Buoyancy Exchange Over the Deglaciation

Most of the decrease in salinity of the MOW over the deglaciation occurs during HS1, presumably during H1.2 when both the stable isotope and grain size data record significant changes. Another significant decrease in salinity of approximately four units occurs during S1. A decrease in salinity can indicate both a change in MOW strength and a change in the location of the MOW plume, both lateral and vertical. In this section we evaluate both possibilities over the deglaciation starting with the decrease in salinity during HS1.

Deep water temperatures drop to approximately 2°C at the transition from H1.1 to H1.2 (Figure 6a). Similar drops in DWT occur during B/A and S1. The three cold spells over the deglaciation can represent periods when MOW was absent or weak and was replaced by cold (glacial) NADW or Antarctic Intermediate Water. At these times we also record a reduction in the abundance of the coarse grain size fraction (Figure 6f). Specifically, the coarse-grained size fraction indicates that MOW strength decreases during H1.1 and then rapidly increases at the end of H1.2 at 1,000 m depth simultaneous with a rapid increase in DWT to 13°C. The increase in the coarse-grained fraction (>63 μm) in the late phase of HS1 is also recorded at Site MD99-2339 in the Gulf of Cadiz at 1170 m depth, located approximately 25 km south of Site U1390 (Voelker et al., 2006). At MD99-2339, the coarse-grained fraction also increases during YD, which is less evident in our record.

Synchronous with the decrease in the DWT and the coarse-grained fraction at the end of H1.2, benthic $\delta^{13}C$ also decreases at sites U1390 and MD99-2339, which is also true for other sites between 820 to 1873 m depth, both within the Gulf of Cadiz and along the Iberian Peninsula, where MOW flows along the seafloor morphology (Schönfeld & Zahn, 2000; Zahn et al., 1987). There are three ways to explain the decrease in benthic $\delta^{13}C$. First, the synchronous drop in benthic $\delta^{13}C$ below 820 m could indicate a lower ventilation of the Mediterranean Sea during that time (Voelker et al., 2006) resulting in the reduction in MOW strength. In this view, the fact that the decrease in benthic $\delta^{13}C$ occurs earlier at Site MD99-2339 than at Site U1390 (Figure 6c) could hint at a lateral change of the MOW plume at this time. The drop in benthic $\delta^{13}C$ can also been explained by a lower ventilation of North Atlantic intermediate waters caused by a reduced AMOC at that time (Zahn et al., 1997). As the AMOC and the MOW are coupled through the Gibraltar exchange, both interpretations can be considered as mutually consistent. Alternatively, the decrease in $\delta^{13}C$ can be explained by the increase in North Atlantic overturning resulting in the upwelling of waters below 4,010 m, which were relatively depleted in ^{13}C (Figure 6d).

Published records of MOW strength document an increase in MOW flux at a depth of approximately 600 m across HS1 and the YD within the Gulf of Cadiz (Bahr et al., 2014, 2015; Llave et al., 2006; Toucanne et al.,

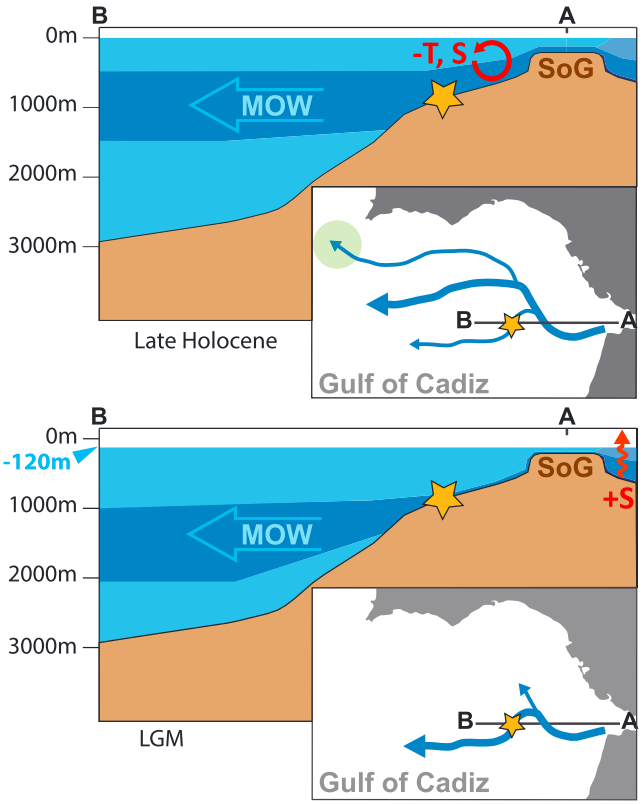

Figure 7. Sketch of the scenario in which the Mediterranean Outflow Water (MOW) plume shoals from the Last Glacial Maximum (LGM) (bottom) toward the Late Holocene (top). The projected 2-D location of Site U1390 is highlighted with the yellow star. During the last glacial lowstand, the Mediterranean was a more evaporative and hence more saline basin. Increasing buoyancy exchange through the Strait of Gibraltar over the deglaciation resulted in more admixing, while the MOW plume shoaled presumably due to a change in the vertical density structure of the North Atlantic. At its new settling depth, the plume possibly became increasingly directed toward the north (modified from Rogerson et al., 2006).

2007). The MOW current presumably shoaled from 1,600–2,200 m to 1,300 m depth over the deglaciation along the Portuguese Iberian Margin (Schönfeld & Zahn, 2000). This shoaling could have been caused by a radical change in the vertical density structure of North Atlantic waters (Baringer & Price, 1997; Rogerson et al., 2005, 2012). A reduction in MOW strength at this time as recorded in our records supports the hypothesized shoaling of the MOW plume. The brief and rapid increase in MOW strength during the later phase of H1.2 at first glance undermines the hypothesized shoaling of the MOW plume. We can hypothesize on the meaning of this increase once we take a closer look at the sequence of events in the central Gulf of Cadiz during HS1.

The salt that had accumulated in the Mediterranean Sea during the glacial low stand presumably surged into the Atlantic during HS1 as evidenced by an increased gradient in planktic δ^{18}O across the Strait of Gibraltar (Rogerson et al., 2010). In fact, record of ice-rafted debris (IRD) show that pulses of North Atlantic meltwater repeatedly arrived east of the Strait of Gibraltar synchronous with increased gradients in planktic δ^{18}O across the Strait of Gibraltar (Rogerson et al., 2010; Toucanne et al., 2007; Voelker et al., 2006). The significant increase in planktic δ^{13}C across HS1 and YD reported here supports a sudden change in surface water conditions at Site U1390 (Figure 3). As the meltwater that arrived in the Gulf of Cadiz was cold (e.g., Voelker et al., 2006) and likely poor in nutrients, primary productivity in the surface waters, and hence planktic δ^{13}C, did not increase as evident from the constant export productivity at Site MD99-2339 during HS1 (Voelker et al., 2009). Hence, we hypothesize that the increase in planktic δ^{13}C is more likely related to the transfer of high δ^{13}C MOW to the surface waters through increased vertical mixing as suggested by the strong coupling of benthic and planktic δ^{13}C during HS1 and the rapid increase in DWT during the later phase of H1.2. A similar coupling of DWT and planktic δ^{13}C is observed during YD.

The strong coupling of both deep and surface dissolved inorganic carbon pools suggests that admixing of MOW with North Atlantic Central water masses increased across HS1. The delay between the Atlantic freshening during H1.1 and the change in MOW properties during H1.2 might be related to an initial reduction in deep water convection and WMDW formation in the Alboran Sea (e.g., Voelker et al., 2006) and Gulf of Lions (Sierro et al., 2005). Alternatively, the freshwater melt and the rise in sea level during H1.1 might not have been significant enough to trigger intensified Atlantic-Mediterranean buoyancy exchange. Perhaps, the negative feedback could only initiate at the arrival of meltwater pulse 1a in the central Gulf of Cadiz at the transition from HS1 into B/A (Deschamps et al., 2012).

Thus, although our age model does not have the optimal resolution to quantitatively decipher submillennial-scale climate variability, our records support the hypothesized loss of MOW salinity and shoaling of the MOW plume at the transition from HS1 into the B/A potentially triggered by the arrival of meltwater pulse 1a in the central Gulf of Cadiz (Reid, 1979; Rogerson et al., 2005, 2006, 2010; Sánchez Goñi et al., 2016; Toucanne et al., 2007; Voelker et al., 2006). Since MOW settling depth can be insensitive to the properties of MOW (Rogerson et al., 2012), it is challenging to precisely disentangle what part of the salinity anomaly presented here is due to shoaling and what part is due to a change in MOW properties or strength. Furthermore, it is challenging to define the fate of the recorded decrease in MOW salinity across H1.2. The increased buoyancy exchange across the Strait of Gibraltar (e.g., Rogerson et al., 2010), decrease in salinity in the deep central Gulf of Cadiz (Figure 6g), and potential shoaling of the MOW plume suggest that admixing with North Atlantic Central water masses increased over the deglaciation (Figure 7), which could explain a slight cooling at Site U1390 as suggested by the clumped isotope-based DWT record (Figure 6a). Furthermore, the shoaling is hypothesized to drive a more northward direction of the MOW plume (Rogerson et al., 2006; Figure 7).

In order to summarize the role of MOW on deglacial North Atlantic circulation, we included records on North Atlantic ventilation, which were discussed briefly before and circulation (Figures 6d and 6e). Combined, these records provide a broader understanding on the potential role of the MOW as a negative feedback on decreased deep water formation in the North Atlantic in three steps. First, the heterogeneity in the $\delta^{13}C$ transects compiled at different depths indicates the poor ventilation of water masses below 2,300 during the LGM (Lisiecki et al., 2008; Figure 6d). Then, Pa/Th records highlight the abrupt drawdown in the strength of North Atlantic overturning at different depths during HS1 related to the meltdown of Northern Hemisphere ice sheets (Gherardi et al., 2005; Roberts et al., 2014; Figure 6e). This meltdown could have been related to the release of heat stored in the deep Nordic Seas during the last glacial period (Thornalley et al., 2015). Finally, in response to the meltwater pulse, buoyancy exchange at the Strait of Gibraltar intensifies under a rapidly rising sea level. Salinity stored during the glacial low stand surges into the Gulf of Cadiz (Figure 6g) and possibly further north while buoyancy exchange continuous through admixing with North Atlantic Central waters. The release of Mediterranean salt is synchronous with increased Agulhas leakage into the North Atlantic (Chiessi et al., 2008; Peeters et al., 2004), which acts as another negative feedback on reduced AMOC (Knorr & Lohmann, 2003; Weijer et al., 2002).

We find a second pronounced decrease in salinity of approximately four units during S1 that coincides with a minimum in DWT and grain size but no change planktic $\delta^{13}C$. Both shallow and deep sites in the Gulf of Cadiz record this minimum in MOW strength (Bahr et al., 2015; Toucanne et al., 2007; Voelker et al., 2006), which likely represents a temporary replacement of MOW by NADW in the central Gulf of Cadiz. MOW might have been more sluggish at this time, due to the well-documented decrease in deep water formation in the Eastern Mediterranean. Synchronous with the displacement of MOW by NADW, the minima in benthic $\delta^{13}C$ at sites U1390 and MD99-2339 possibly capture the decrease in Eastern Mediterranean ventilation leading to the deposition of S1. The salinity anomaly associated with S1 ends at 5.5 ka (Figure 6g). At this time, the MOW plume likely gained its present configuration as evident from deep water velocity reconstructions along the Portuguese margin (Schönfeld & Zahn, 2000).

6. Conclusions

Species-specific differences not only in absolute values but also in terms of variability make it difficult to interpret Mg/Ca-based temperature reconstructions of Mediterranean deep waters. However, the combination of Mg/Ca with Δ_{47} based thermometry on benthic foraminifera provided new insights into evolution of MOW across the last deglaciation. While DWT remained constant, salinity decreased by at least three and possibly up to eight salinity units at IODP Site U1390 (1,000 m depth) from the LGM to the Holocene. These results are in agreement with a much more saline Mediterranean endmember during glacial times. Our findings suggest that the salt that had accumulated during the glacial low stand surged into the North Atlantic in response to North Atlantic freshening during H1.2. At this time MOW was repeatedly replaced by NADW at Site U1390 as recorded by two rapid DWT coolings. A third interval of MOW absence is related to the reduction in deep water formation in the eastern Mediterranean Sea resulting in the deposition of S1.

We propose that the increase in Atlantic-Mediterranean buoyancy exchange during H1.2 could have occurred simultaneously with a shoaling in the MOW plume although more high-resolution $\delta^{18}O_w$ reconstructions and improved understanding of the salinity/$\delta^{18}O_w$ proxy are essential to confirm this. Our findings support the hypothesis that the MOW acts as a negative feedback system to freshening events in the North Atlantic across the last deglaciation.

Acknowledgments
The supporting information are available at https://doi.org/10.1594/PANGAEA.884623 and as a supplement to this publication. We are greatly indebted to the IODP Expedition Party 339 for support onboard the DV Joides Resolution. We acknowledge Mike Rogerson, Stefanie Kaboth, and Francisco J. Sierro for sharing their expertise on the Gibraltar exchange. Furthermore, we are grateful for the expert assistance during measurements of Wim Boer (NIOZ), Stewart Bishop (ETHZ), and Madalina Jäggi (ETHZ). We acknowledge the French Artemis program of the Institut National des Sciences de l'Univers and the Keck Carbon Cycle AMS facility at the University of California, Irvine, for the AMS ^{14}C datings. We are grateful for the comments of three anonymous reviewers, Michael Sarnthein, and Antje Voelker, which improved the manuscript significantly. Funding was received through EU FP7 Marie Curie grant 298513, ETH grant 33 14-1, and NWO-ALW grant 865.10.001.

References

Aït-Ameur, N., & Goyet, C. (2006). Distribution and transport of natural and anthropogenic CO_2 in the Gulf of Cádiz. *Deep Sea Research Part II: Topical Studies in Oceanography*, *53*, 1329–1343. https://doi.org/10.1016/j.dsr2.2006.04.003

Ambar, I., & Howe, M. R. (1979). Observations of the Mediterranean outflow—I. Mixing in the Mediterranean outflow. *Deep Sea Research Part A: Oceanographic Research Papers*, *26*(5), 535–554. https://doi.org/10.1016/0198-0149(79)90095-5

Ambar, I., Serra, N., Brogueira, M. J., Cabeçadas, G., Abrantes, F., Freitas, P., … Gonzalez, N. (2002). Physical, chemical and sedimentological aspects of the Mediterranean outflow off Iberia. *Deep Sea Research Part II: Topical Studies in Oceanography*, *49*(19), 4163–4177. https://doi.org/10.1016/S0967-0645(02)00148-0

Austermann, J., Mitrovica, J. X., Latychev, K., & Milne, G. A. (2013). Barbados-based estimate of ice volume at Last Glacial Maximum affected by subducted plate. *Nature Geoscience*, *6*(7), 553–557. https://doi.org/10.1038/ngeo1859

Bahr, A., Jiménez-Espejo, F. J., Kolasinac, N., Grunert, P., Hernández-Molina, F. J., Röhl, U., … Alvarez-Zarikian, C. A. (2014). Deciphering bottom current velocity and paleoclimate signals from contourite deposits in the Gulf of Cádiz during the last 140 kyr: An inorganic geochemical approach. *Geochemistry, Geophysics, Geosystems*, *15*, 3145–3160. https://doi.org/10.1002/2014GC005356

Bahr, A., Kaboth, S., Jiménez-Espejo, F. J., Sierro, F. J., Voelker, A. H. L., Lourens, L., … Friedrich, O. (2015). Persistent monsoonal forcing of Mediterranean outflow water dynamics during the late Pleistocene. *Geology*, *43*(11), 951–954. https://doi.org/10.1130/G37013.1

Baringer, M. O., & Price, J. F. (1997). Mixing and spreading of the Mediterranean outflow. *Journal of Physical Oceanography*, *27*(8), 1654–1677. https://doi.org/10.1175/1520-0485(1997)027%3C1654:MASOTM%3E2.0.CO;2

Barker, S., Greaves, M., & Elderfield, H. (2003). A study of cleaning procedures used for foraminiferal Mg/Ca paleothermometry. *Geochemistry, Geophysics, Geosystems*, *4*(9), 8407. https://doi.org/10.1029/2003GC000559

Bigg, G. R. (1995). Aridity of the Mediterranean Sea at the Last Glacial Maximum: A reinterpretation of the δ^{18}O record. *Paleoceanography*, *10*(2), 283–290. https://doi.org/10.1029/94PA03165

Bigg, G. R., & Wadley, M. R. (2001). Millennial-scale variability in the oceans: An ocean modelling view. *Journal of Quaternary Science*, *16*(4), 309–319. https://doi.org/10.1002/jqs.599

Bigg, G. R., Jickells, T. D., Liss, P. S., & Osborn, T. J. (2003). The role of the oceans in climate. *International Journal of Climatology*, *23*(10), 1127–1159. https://doi.org/10.1002/joc.926

Borenäs, K. M., Wahlin, A. K., Ambar, I., & Serra, N. (2002). The Mediterranean outflow splitting—A comparison between theoretical models and CANIGO data. *Deep Sea Research Part II: Topical Studies in Oceanography*, *49*(19), 4195–4205. https://doi.org/10.1016/S0967-0645(02)00150-9

Brambilla, E., Talley, L. D., & Robbins, P. E. (2008). Subpolar mode water in the northeastern Atlantic: 2. Origin and transformation. *Journal of Geophysical Research*, *113*, C04026. https://doi.org/10.1029/2006JC004063

Breitenbach, S. F. M., & Bernasconi, S. M. (2011). Carbon and oxygen isotope analysis of small carbonate samples (20 to 100 μg) with a GasBench II preparation device. *Rapid Communications in Mass Spectrometry*, *25*, 1910–1914. https://doi.org/10.1002/rcm.5052

Cabeçadas, G., José Brogueira, M., & Gonçalves, C. (2002). The chemistry of Mediterranean outflow and its interactions with surrounding waters. *Deep Sea Research Part II: Topical Studies in Oceanography*, *49*(19), 4263–4270. https://doi.org/10.1016/S0967-0645(02)00154-6

Cacho, I., Shackleton, N., Elderfield, H., Sierro, F. J., & Grimalt, J. O. (2006). Glacial rapid variability in deep-water temperature and δ^{18}O from the Western Mediterranean Sea. *Quaternary Science Reviews*, *25*, 3294–3311. https://doi.org/10.1016/j.quascirev.2006.10.004

Chiessi, C. M., Mulitza, S., Paul, A., Pätzold, J., Groeneveld, J., & Wefer, G. (2008). South Atlantic interocean exchange as the trigger for the Bøolling warm event. *Geology*, *36*, 919–922. https://doi.org/10.1130/G24979A.1

Cramp, A., & O'Sullivan, G. (1999). Neogene sapropels in the Mediterranean: A review. *Marine Geology*, *153*(1–4), 11–28. https://doi.org/10.1016/S0025-3227(98)00092-9

De Lange, G. J., Thomson, J., Reitz, A., Slomp, C. P., Speranza Principato, M., Erba, E., & Corselli, C. (2008). Synchronous basin-wide formation and redox-controlled preservation of a Mediterranean sapropel. *Nature Geoscience*, *1*, 606–610. https://doi.org/10.1038/ngeo283

Dennis, K. J., Affek, H. P., Passey, B. H., Schrag, D. P., & Eiler, J. M. (2011). Defining an absolute reference frame for "clumped" isotope studies of CO_2. *Geochimica et Cosmochimica Acta*, *75*, 7117–7131. https://doi.org/10.1016/j.gca.2011.09.025

Deschamps, P., Durand, N., Bard, E., Hamelin, B., Camoin, G., Thomas, A. L., … Yokoyama, Y. (2012). Ice-sheet collapse and sea-level rise at the Bølling warming 14,600 years ago. *Nature*, *483*, 559–564. https://doi.org/10.1038/nature10902

Dueñas-Bohórquez, A., da Rocha, R. E., Kuroyanagi, A., Bijma, J., & Reichart, G. J. (2009). Effect of salinity and seawater calcite saturation state on Mg and Sr incorporation in cultured planktonic foraminifera. *Marine Micropaleontology*, *73*, 178–189. https://doi.org/10.1016/j.marmicro.2009.09.002

Dueñas-Bohórquez, A., Raitzsch, M., de Nooijer, L. J., & Reichart, G. J. (2011). Independent impacts of calcium and carbonate ion concentration on Mg and Sr incorporation in cultured benthic foraminifera. *Marine Micropaleontology*, *81*, 122–130. https://doi.org/10.1016/j.marmicro.2011.08.002

Elderfield, H., Yu, J., Anand, P., Kiefer, T., & Nyland, B. (2006). Calibrations for benthic foraminiferal Mg/Ca paleothermometry and the carbonate ion hypothesis. *Earth and Planetary Science Letters*, *250*, 633–649. https://doi.org/10.1016/j.epsl.2006.07.041

Elderfield, H., Greaves, M., Barker, S., Hall, I. R., Tripati, A., Ferretti, P., … Daunt, C. (2010). A record of bottom water temperature and seawater δ^{18}O for the Southern Ocean over the past 440 kyr based on Mg/Ca of benthic foraminiferal Uvigerina spp. *Quaternary Science Reviews*, *29*, 160–169. https://doi.org/10.1016/j.quascirev.2009.07.013

Fairbanks, R. G. (1989). A 17,000-year glacio-eustatic sea level record: influence of glacial melting rates on the Younger Dryas event and deep-ocean circulation. *Nature*, *342*(6250), 637–642. https://doi.org/10.1038/342637a0

Faugères, J. C., Gonthier, E., & Stow, D. A. V. (1984). Contourite drift molded by deep Mediterranean outflow. *Geology*, *12*(5), 296–300. https://doi.org/10.1130/0091-7613(1984)12%3C296:CDMBDM%3E2.0.CO;2

Fernandez, A., Müller, I. A., Rodríguez-Sanz, L., van Dijk, J., Looser, N., & Bernasconi, S. M. (2018). A reassessment of the precision of carbonate clumped isotope measurements: implications for calibrations and paleoclimate reconstructions. *Geochemistry, Geophysics, Geosystems*, *18*, 4375–4386, https://doi.org/10.1002/2017GC007106

Fiúza, A. F. G., Hamann, M., Ambar, I., Díaz Del Río, G., González, N., & Cabanas, J. M. (1998). Water masses and their circulation off western Iberia during May 1993. *Deep Sea Research Part I: Oceanographic Research Papers*, *45*(7), 1127–1160. https://doi.org/10.1016/S0967-0637(98)00008-9

Fletcher, W. J., Sanchez Goñi, M. F., Peyron, O., & Dormoy, I. (2009). Abrupt climate changes of the last deglaciation detected in a western Mediterranean forest record. *Climate of the Past Discussions*, *5*, 203–235. https://doi.org/10.5194/cpd-5-203-2009

Fontanier, C., MacKensen, A., Jorissen, F. J., Anschutz, P., Licari, L., & Griveaud, C. (2006). Stable oxygen and carbon isotopes of live benthic foraminifera from the Bay of Biscay: Microhabitat impact and seasonal variability. *Marine Micropaleontology*, *58*, 159–183. https://doi.org/10.1016/j.marmicro.2005.09.004

Gherardi, J. M., Labeyrie, L., McManus, J. F., Francois, R., Skinner, L. C., & Cortijo, E. (2005). Evidence from the Northeastern Atlantic basin for variability in the rate of the meridional overturning circulation through the last deglaciation. *Earth and Planetary Science Letters*, *240*, 710–723. https://doi.org/10.1016/j.epsl.2005.09.061

Ghosh, P., Adkins, J., Affek, H., Balta, B., Guo, W., Schauble, E. A., … Eiler, J. M. (2006). ^{13}C-^{18}O bonds in carbonate minerals: A new kind of paleothermometer. *Geochimica et Cosmochimica Acta*, *70*, 1439–1456. https://doi.org/10.1016/j.gca.2005.11.014

Grauel, A. L., Schmid, T. W., Hu, B., Bergami, C., Capotondi, L., Zhou, L., & Bernasconi, S. M. (2013). Calibration and application of the "clumped isotope" thermometer to foraminifera for high-resolution climate reconstructions. *Geochimica et Cosmochimica Acta*, *108*, 125–140. https://doi.org/10.1016/j.gca.2012.12.049

Groeneveld, J., Nürnberg, D., Tiedemann, R., Reichart, G. J., Steph, S., Reuning, L., … Mason, P. (2008). Foraminiferal Mg/Ca increase in the Caribbean during the Pliocene: Western Atlantic Warm Pool formation, salinity influence, or diagenetic overprint? *Geochemistry, Geophysics, Geosystems*, *9*, Q01P23. https://doi.org/10.1029/2006GC001564

Habgood, E. L., Kenyon, N. H., Masson, D. G., Akhmetzhanov, A., Weaver, P. P. P. E., Gardner, J., & Mulder, T. (2003). Deep-water sediment wave fields, bottom current sand channels and gravity flow channel-lobe systems: Gulf of Cadiz, NE Atlantic. *Sedimentology*, *50*(3), 483–510. https://doi.org/10.1046/j.1365-3091.2003.00561.x

Henkes, G. A., Passey, B. H., Wanamaker, A. D., Grossman, E. L., Ambrose, W. G., & Carroll, M. L. (2013). Carbonate clumped isotope compositions of modern marine mollusk and brachiopod shells. *Geochimica et Cosmochimica Acta*, *106*, 307–325. https://doi.org/10.1016/j.gca.2012.12.020

Hernández-Molina, F. J., Stow, D., Alvarez-Zarikian, C., & Expedition IODP 339 Scientists (2013). IODP Expedition 339 in the Gulf of Cadiz and off West Iberia: decoding the environmental significance of the Mediterranean outflow water and its global influence. *Scientific Drilling*, *16*, 1–11. https://doi.org/10.5194/sd-16-1-2013

Hernández-Molina, F. J., Stow, D. A., Alvarez-Zarikian, C. A., Acton, G., Bahr, A., Balestra, B., … Xuan, C. (2014). Paleoceanography. Onset of Mediterranean outflow into the North Atlantic. *Science*, *344*(6189), 1244–1250. https://doi.org/10.1126/science.1251306

Hodell, D. A., Nicholl, J. A., Bontognali, T. R. R., Danino, S., Dorador, J., Dowdeswell, J. A., … Röhl, U. (2017). Anatomy of Heinrich layer 1 and its ole in the last deglaciation. *Paleoceanography*, *32*, 284–303. https://doi.org/10.1002/2016PA003028

Holloway, M. D., Sime, L. C., Singarayer, J. S., Tindall, J. C., & Valdes, P. J. (2015). Reconstructing paleosalinity from δ^{18}O: Coupled model simulations of the Last Glacial Maximum, Last Interglacial and Late Holocene. *Quaternary Science Reviews*, *131*, 1–15. https://doi.org/10.1016/j.quascirev.2015.07.007

Hu, A., Meehl, G. A., Han, W., & Yin, J. (2009). Transient response of the MOC and climate to potential melting of the Greenland Ice Sheet in the 21st century. *Geophysical Research Letters*, *36*, L10707. https://doi.org/10.1029/2009GL037998

Iorga, M. C., & Lozier, M. S. (1999). Signatures of the Mediterranean outflow from a North Atlantic climatology: 1. Salinity and density fields. *Journal of Geophysical Research*, *104*(C11), 25,985–26,009. https://doi.org/10.1029/1999JC900115

Ivanovic, R. F., Valdes, P. J., Gregoire, L., Flecker, R., & Gutjahr, M. (2014). Sensitivity of modern climate to the presence, strength and salinity of Mediterranean-Atlantic exchange in a global general circulation model. *Climate Dynamics*, *42*(3–4), 859–877. https://doi.org/10.1007/s00382-013-1680-5

Jorissen, F. J., de Stigter, H. C., & Widmark, J. G. (1995). A conceptual model explaining benthic foraminiferal microhabitats. *Marine Micropaleontology*, *26*(1–4), 3–15.

Jiménez-Espejo, F. J., Pardos-Gené, M., Martínez-Ruiz, F., García-Alix, A., van de Flierdt, T., Toyofuku, T., … Kreissig, K. (2015). Geochemical evidence for intermediate water circulation in the westernmost Mediterranean over the last 20 kyr BP and its impact on the Mediterranean Outflow. *Global and Planetary Change*, *135*, 38–46. https://doi.org/10.1016/j.gloplacha.2015.10.001

Kele, S., Breitenbach, S. F. M., Capezzuoli, E., Meckler, A. N., Ziegler, M., Millan, I. M., … Bernasconi, S. M. (2015). Temperature dependence of oxygen- and clumped isotope fractionation in carbonates: A study of travertines and tufas in the 6–95°C temperature range. *Geochimica et Cosmochimica Acta*, *168*, 172–192. https://doi.org/10.1016/j.gca.2015.06.032

Key, R. M., Olsen, A., van Heuven, S., Lauvset, S. K., Velo, A., Lin, X., … Jutterström, S. (2015). Global Ocean Data Analysis Project, Version 2 (GLODAPv2).

Khélifi, N., Sarnthein, M., Andersen, N., Blanz, T., Frank, M., Garbe-Schönberg, D., … Weinelt, M. (2009). A major and long-term Pliocene intensification of the Mediterranean outflow, 3.5–3.3 Ma ago. *Geology*, *37*, 811–814. https://doi.org/10.1130/G30058A.1

Kim, S. T., O'Neil, J. R., Hillaire-Marcel, C., & Mucci, A. (2007). Oxygen isotope fractionation between synthetic aragonite and water: Influence of temperature and Mg^{2+} concentration. *Geochimica et Cosmochimica Acta*, *71*, 4704–4715. https://doi.org/10.1016/j.gca.2007.04.019

Knorr, G., & Lohmann, G. (2003). Southern Ocean origin for the resumption of Atlantic thermohaline circulation during deglaciation. *Nature*, *424*(6948), 532–536. https://doi.org/10.1038/nature01855

Lea, D. W., Mashiotta, T. A., & Spero, H. J. (1999). Controls on magnesium and strontium uptake in planktonic foraminifera determined by live culturing. *Geochimica et Cosmochimica Acta*, *63*(16), 2369–2379. https://doi.org/10.1016/S0016-7037(99)00197-0

Lear, C. H. (2000). Cenozoic deep-sea temperatures and global ice volumes from Mg/Ca in benthic foraminiferal calcite. *Science*, *287*(5451), 269–272. https://doi.org/10.1126/science.287.5451.269

Legrande, A. N., & Schmidt, G. A. (2011). Water isotopologues as a quantitative paleosalinity proxy. *Paleoceanography*, *26*, PA3225. https://doi.org/10.1029/2010PA002043

Linke, P., & Lutze, G. F. (1993). Microhabitat preferences of benthic foraminifera—A static concept or a dynamic adaptation to optimize food acquisition? *Marine Micropaleontology*, *20*(3–4), 215–234. https://doi.org/10.1016/0377-8398(93)90034-U

Lisiecki, L. E., Raymo, M. E., & Curry, W. B. (2008). Atlantic overturning responses to Late Pleistocene climate forcings. *Nature*, *456*, 85–88. https://doi.org/10.1038/nature07425

Llave, E., Schönfeld, J., Hernández-Molina, F. J., Mulder, T., Somoza, L., Díaz Del Río, V., & Sänchez-Almazo, I. (2006). High-resolution stratigraphy of the Mediterranean outflow contourite system in the Gulf of Cadiz during the late Pleistocene: The impact of Heinrich events. *Marine Geology*, *227*, 241–262. https://doi.org/10.1016/j.margeo.2005.11.015

Lo Giudice Cappelli, E., Regenberg, M., Holbourn, A., Kuhnt, W., Garbe-Schönberg, D., & Andersen, N. (2015). Refining C. wuellerstorfi and H. elegans Mg/Ca temperature calibrations. *Marine Micropaleontology*, *121*, 70–84. https://doi.org/10.1016/j.marmicro.2015.10.001

Locarnini, R. A., Mishonov, A. V., Antonov, J. I., Boyer, T. P., Garcia, H. E., Baranova, O. K., … Seidov, D. (2013). World Ocean Atlas 2013, Volume 1: Temperature. In S. Levitus & A. Mishonov (Eds.), *NOAA Atlas NESDIS 73* (40 pp.). https://doi.org/10.1182/blood-2011-06-357442

Lozier, M. S., & Stewart, N. M. (2008). On the temporally varying northward penetration of Mediterranean overflow water and eastward penetration of Labrador Sea water. *Journal of Physical Oceanography*, *38*, 2097–2103. https://doi.org/10.1175/2008JPO3908.1

Lynch-Stieglitz, J., Schmidt, M. W., & Curry, W. B. (2011). Evidence from the Florida Straits for Younger Dryas ocean circulation changes. *Paleoceanography*, *26*, PA1205. https://doi.org/10.1029/2010PA002032

Marchitto, T. M., Curry, W. B., Lynch-Stieglitz, J., Bryan, S. P., Cobb, K. M., & Lund, D. C. (2014). Improved oxygen isotope temperature calibrations for cosmopolitan benthic foraminifera. *Geochimica et Cosmochimica Acta*, *130*, 1–11. https://doi.org/10.1016/j.gca.2013.12.034

Matthiesen, S., & Haines, K. (2003). A hydraulic box model study of the Mediterranean response to postglacial sea-level rise. *Paleoceanography*, *18*(4), 1084. https://doi.org/10.1029/2003PA000880

McCartney, M. S., & Mauritzen, C. (2001). On the origin of the warm inflow to the Nordic Seas. *Progress in Oceanography*, *51*(1), 125–214. https://doi.org/10.1016/S0079-6611(01)00084-2

McManus, J. F., Francois, R., Gherardi, J.-M., Keigwin, L. D., & Brown-Leger, S. (2004). Collapse and rapid resumption of Atlantic meridional circulation linked to deglacial climate changes. *Nature*, *428*, 834–837. https://doi.org/10.1038/nature02494

Meckler, A. N., Ziegler, M., Millán, M. I., Breitenbach, S. F. M., & Bernasconi, S. M. (2014). Long-term performance of the Kiel carbonate device with a new correction scheme for clumped isotope measurements. *Rapid Communications in Mass Spectrometry*, *28*(15), 1705–1715. https://doi.org/10.1002/rcm.6949

Millot, C., Candela, J., Fuda, J. L., & Tber, Y. (2006). Large warming and salinification of the Mediterranean outflow due to changes in its composition. *Deep Sea Research Part I: Oceanographic Research Papers*, *53*, 656–666. https://doi.org/10.1016/j.dsr.2005.12.017

Mook, W. G., & van der Plicht, J. (1999). Reporting ^{14}C activities and concentrations. *Radiocarbon*, *41*(3), 227–239.

Myers, P. G., Haines, K., & Rohling, E. J. (1998). Modeling the paleocirculation of the Mediterranean: The Last Glacial Maximum and the Holocene with emphasis on the formation of sapropel S1. *Paleoceanography*, *13*(6), 586–606. https://doi.org/10.1029/98PA02736

New, A. L., Barnard, S., Herrmann, P., & Molines, J. M. (2001). On the origin and pathway of the saline inflow to the Nordic Seas: Insights from models. *Progress in Oceanography*, *48*(2–3), 255–287. https://doi.org/10.1016/S0079-6611(01)00007-6

Nürnberg, D. (1995). Magnesium in tests of Neogloboquadrina pachyderma sinistral from high northern and southern latitudes. *Journal of Foraminiferal Research*, *25*(4), 350–368. https://doi.org/10.2113/gsjfr.25.4.350

Nürnberg, D., Bijma, J., & Hemleben, C. (1996). Assessing the reliability of magnesium in foraminiferal calcite as a proxy for water mass temperatures. *Geochimica et Cosmochimica Acta*, *60*(5), 803–814. https://doi.org/10.1016/0016-7037(95)00446-7

Okai, T., Suzuki, A., & Kawahata, H. (2001). Preparation of a new geological survey of Japan geochemical reference material: Coral JCp-1. *Geostandards Newsletter*, *26*, 95–99.

Paul, H. A., Bernasconi, S. M., Schmid, D. W., & McKenzie, J. A. (2001). Oxygen isotope composition of the Mediterranean Sea since the Last Glacial Maximum: Constraints from pore water analyses. *Earth and Planetary Science Letters*, *192*(1), 1–14. https://doi.org/10.1016/S0012-821X(01)00437-X

Peeters, F. J. C., Acheson, R., Brummer, G.-J. A., de Ruijter, W. P. M., Schneider, R. R., Ganssen, G. M., … Kroon, D. (2004). Vigorous exchange between the Indian and Atlantic oceans at the end of the past five glacial periods. *Nature*, *430*, 661–665. https://doi.org/10.1038/nature02785

Pierre, C. (1999). The oxygen and carbon isotope distribution in the Mediterranean water masses. *Marine Geology*, *153*(1–4), 41–55. https://doi.org/10.1016/S0025-3227(98)00090-5

Price, J., & Yang, J. (1998). Marginal sea overflows for climate simulations. *Ocean Modeling and Parameterization* (Vol. 516, pp. 155–170). Dordrecht: Springer.

Rahmstorf, S. (1998). Influence of Mediterranean Outflow on climate. *Eos (Washington. DC).*, *79*(24), 281–282. https://doi.org/10.1029/98EO00218

Raitzsch, M., Kuhnert, H., Groeneveld, J., & Bickert, T. (2008). Benthic foraminifer Mg/Ca anomalies in South Atlantic core top sediments and their implications for paleothermometry. *Geochemistry, Geophysics, Geosystems*, *9*, Q05010. https://doi.org/10.1029/2007GC001788

Reid, J. L. (1979). On the contribution of the Mediterranean Sea outflow to the Norwegian-Greenland Sea. *Deep Sea Research Part A: Oceanographic Research Papers*, *26*(11), 1199–1223. https://doi.org/10.1016/0198-0149(79)90064-5

Reimer, P. J., Bard, E., Bayliss, A., Beck, J. W., Blackwell, P. G., Ramsey, C. B., … Grootes, P. M. (2013). IntCal13 and Marine13 radiocarbon age calibration curves 0–50,000 years cal BP. *Radiocarbon*, *55*(4), 1869–1887.

Roberts, N. L., McManus, J. F., Piotrowski, A. M., & McCave, I. N. (2014). Advection and scavenging controls of Pa/Th in the northern NE Atlantic. *Paleoceanography*, *29*, 668–679. https://doi.org/10.1002/2014PA002633

Rogerson, M., Rohling, E. J., Weaver, P. P. E., & Murray, J. W. (2005). Glacial to interglacial changes in the settling depth of the Mediterranean Outflow plume. *Paleoceanography*, *20*, PA3007. https://doi.org/10.1029/2004PA001106

Rogerson, M., Rohling, E. J., & Weaver, P. P. E. (2006). Promotion of meridional overturning by Mediterranean-derived salt during the last deglaciation. *Paleoceanography*, *21*, PA4101. https://doi.org/10.1029/2006PA001306

Rogerson, M., Colmenero-Hidalgo, E., Levine, R. C., Rohling, E. J., Voelker, A. H. L., Bigg, G. R., … Garrick, K. (2010). Enhanced Mediterranean-Atlantic exchange during Atlantic freshening phases. *Geochemistry, Geophysics, Geosystems*, *11*, Q08013. https://doi.org/10.1029/2009GC002931

Rogerson, M., Bigg, G. R., Rohling, E. J., & Ramirez, J. (2012). Vertical density gradient in the eastern North Atlantic during the last 30,000 years. *Climate Dynamics*, *39*(3), 589–598. https://doi.org/10.1007/s00382-011-1148-4

Rohling, E. J. (1999). Environmental control on Mediterranean salinity and $\delta^{18}O$. *Paleoceanography*, *14*(6), 706–715. https://doi.org/10.1029/1999PA900042

Rohling, E. J. (2007). Progress in paleosalinity: Overview and presentation of a new approach. *Paleoceanography*, *22*, PA3215. https://doi.org/10.1029/2007PA001437

Rohling, E. J., & De Rijk, S. (1999). Holocene climate optimum and Last Glacial Maximum in the Mediterranean: The marine oxygen isotope record. *Marine Geology*, *153*(1–4), 57–75. https://doi.org/10.1016/S0025-3227(98)00020-6

Russell, A. D., Hönisch, B., Spero, H. J., & Lea, D. W. (2004). Effects of seawater carbonate ion concentration and temperature on shell U, Mg, and Sr in cultured planktonic foraminifera. *Geochimica et Cosmochimica Acta*, *68*, 4347–4361. https://doi.org/10.1016/j.gca.2004.03.013

Sánchez Goñi, M. F., Llave, E., Oliveira, D., Naughton, F., Desprat, S., Ducassou, E., … Hernández-Molina, F. J. (2016). Climate changes in south western Iberia and Mediterranean Outflow variations during two contrasting cycles of the last 1 Myrs: MIS 31-MIS 30 and MIS 12-MIS 11. *Global and Planetary Change*, *136*, 18–29. https://doi.org/10.1016/j.gloplacha.2015.11.006

Schlitzer, R. (2017). Ocean Data View, odv.awi.de

Schönfeld, J., & Zahn, R. (2000). Late Glacial to Holocene history of the Mediterranean outflow. Evidence from benthic foraminiferal assemblages and stable isotopes at the Portuguese margin. *Palaeogeography Palaeoclimatology Palaeoecology*, *159*(1–2), 85–111. https://doi.org/10.1016/S0031-0182(00)00035-3

Shackleton, N. J. (1974). Attainment of isotopic equilibrium between ocean water and the benthonic foraminifera geuns *Uvigerina*: Isotopic changes in the ocean during the last glacial. *Colloques Internationaux du Centre National de la Recherche Scientifique*, *219*, 203–210.

Sierro, F. J., Hodell, D. A., Curtis, J. H., Flores, J. A., Reguera, I., Colmenero-Hidalgo, E., … Canals, M. (2005). Impact of iceberg melting on Mediterranean thermohaline circulation during Heinrich events. *Paleoceanography*, *20*, PA2019. https://doi.org/10.1029/2004PA001051

Steffensen, J. P., Andersen, K. K., Bigler, M., Clausen, H. B., Dahl-Jensen, D., Fischer, H., … White, J. W. C. (2008). High-resolution Greenland ice core data show abrupt climate change happens in few years. *Science*, *321*(5889), 680–684. https://doi.org/10.1126/science.1157707

Stow, D. A. V., Hernández-Molina, F. J., Alvarez-Zarikian, C. A., & the Expedition 339 Scientists (2013). Site U1390. *Proceedings of the Integrated Ocean Drilling Program*, *339*. Tokyo (Integrated Ocean Drilling Program Management International, Inc.). https://doi.org/10.2204/iodp.proc.339.108.2013

Stuiver, M., Reimer, P. J., & Reimer, R. W. (2017). CALIB 7.0.4 [WWW program] at http://calib.org

Thornalley, D. J. R., Bauch, H. A., Gebbie, G., Guo, W., Ziegler, M., Bernasconi, S. M., … Yu, J. (2015). A warm and poorly ventilated deep Arctic Mediterranean during the last glacial period. *Science*, *349*(6249), 706–710. https://doi.org/10.1126/science.aaa9554

Toucanne, S., Mulder, T., Schönfeld, J., Hanquiez, V., Gonthier, E., Duprat, J., … Zaragosi, S. (2007). Contourites of the Gulf of Cadiz: A high-resolution record of the paleocirculation of the Mediterranean outflow water during the last 50,000??years. *Palaeogeography Palaeoclimatology Palaeoecology*, *246*(2–4), 354–366. https://doi.org/10.1016/j.palaeo.2006.10.007

Toucanne, S., Jouet, G., Ducassou, E., Bassetti, M. A., Dennielou, B., Angue Minto'o, C. M., … Mulder, T. (2012). A 130,000-year record of Levantine Intermediate Water flow variability in the Corsica Trough, western Mediterranean Sea. *Quaternary Science Reviews*, *33*, 55–73. https://doi.org/10.1016/j.quascirev.2011.11.020

Tripati, A. K., Eagle, R. A., Thiagarajan, N., Gagnon, A. C., Bauch, H., Halloran, P. R., & Eiler, J. M. (2010). ^{13}C-^{18}O isotope signatures and "clumped isotope" thermometry in foraminifera and coccoliths. *Geochimica et Cosmochimica Acta*, *74*(20), 5697–5717. https://doi.org/10.1016/j.gca.2010.07.006

Voelker, A. H. L., Lebreiro, S. M., Schönfeld, J., Cacho, I., Erlenkeuser, H., & Abrantes, F. (2006). Mediterranean outflow strengthening during northern hemisphere coolings: A salt source for the glacial Atlantic? *Earth and Planetary Science Letters*, *245*, 39–55. https://doi.org/10.1016/j.epsl.2006.03.014

Voelker, A. H. L., De Abreu, L., Schönfeld, J., Erlenkeuser, H., & Abrantes, F. (2009). Hydrographic conditions along the western Iberian margin during marine isotope stage 2. *Geochemistry, Geophysics, Geosystems*, *10*, Q12U08. https://doi.org/10.1029/2009GC002605

Voelker, A. H. L., Colman, A., Olack, G., Waniek, J. J., & Hodell, D. (2015). Oxygen and hydrogen isotope signatures of Northeast Atlantic water masses. *Deep Sea Research Part II: Topical Studies in Oceanography*, *116*, 89–106. https://doi.org/10.1016/j.dsr2.2014.11.006

Waelbroeck, C., Labeyrie, L., Michel, E., Duplessy, J. C., McManus, J. F., Lambeck, K., … Labracherie, M. (2002). Sea-level and deep water temperature changes derived from benthic foraminifera isotopic records. *Quaternary Science Reviews*, *21*(1–3), 295–305. https://doi.org/10.1016/S0277-3791(01)00101-9

Wefer, G., & Mulitza, S. (2004). *The South Atlantic in the late Quaternary: Reconstruction of materials budgets and current systems*. Springer Science & Business Media.

Weijer, W., De Ruijter, W. P. M., Sterl, A., & Drijfhout, S. S. (2002). Response of the Atlantic overturning circulation to South Atlantic sources of buoyancy. *Global and Planetary Change*, *34*(3–4), 293–311. https://doi.org/10.1016/S0921-8181(02)00121-2

Wu, W., Danabasoglu, G., & Large, W. G. (2007). On the effects of parameterized Mediterranean overflow on North Atlantic ocean circulation and climate. *Ocean Modelling*, *19*, 31–52. https://doi.org/10.1016/j.ocemod.2007.06.003

Zahn, R., Sarnthein, M., & Erlenkeuser, H. (1987). Benthic isotope evidence for changes of the Mediterranean outflow during the late Quaternary. *Paleoceanography*, *2*(6), 543–559.

Zahn, R., Schönfeld, J., Kudrass, H. R., Park, M. H., Erlenkeuser, H., & Grootes, P. (1997). Thermohaline instability in the North Atlantic during melt water events: Stable isotope and ice-rafted detritus records from core SO75-26KL, Portuguese margin. *Paleoceanography*, *12*(5), 696–710. https://doi.org/10.1029/97PA00581

Zweng, M. M., Reagan, J. R., Antonov, J. I., Mishonov, A. V., Boyer, T. P., Garcia, H. E., … Bidlle, M. M. (2013). World Ocean Atlas 2013, Volume 2: Salinity. *NOAA Atlas NESDIS*, *2*(1), 39. https://doi.org/10.1182/blood-2011-06-357442